

Contents lists available at [ScienceDirect](https://www.sciencedirect.com)

International Journal of Rock Mechanics and Mining Sciences

journal homepage: www.elsevier.com/locate/ijmms

Anisotropic deformability and strength of slate from NW-Spain

L.R. Alejano^{a,*}, M.A. González-Fernández^a, X. Estévez-Ventosa^a, Fei Song^b,
J. Delgado-Martín^c, A. Muñoz-Ibáñez^c, N. González-Molano^d, J. Alvarellos^d^a CINTECX, University of Vigo, GESSMin Group, Department of Natural Resources and Environmental Engineering, Vigo, Spain^b Department of Civil and Environmental Engineering, Politechnic University of Catalonia, Barcelona, Spain^c Department of Civil Engineering, University of La Coruña, Spain^d Repsol Technology Lab, Móstoles, Madrid, Spain

ARTICLE INFO

Keywords:

Slate
Anisotropy
Transversely isotropic elasticity
Strength
JPW

ABSTRACT

Slates are metamorphic rocks characterized by the pervasive occurrence of cleavage or foliation producing a highly anisotropic mechanical behavior characterized by fissility. Deformability and strength of these rocks are therefore dependent on the cleavage plane orientations relative to the principal stresses. In this study, the failure and deformability of these rocks are experimentally investigated by means of a set of standard uniaxial and triaxial compression tests on samples cut with the cleavage forming different angles. Propagation velocity measurements have also been taken in a good number of specimens. Compression tests show that deformability and strength are clearly anisotropic for this rock and that failure through the cleavage plane is observed in the range of dip angles from 15 to 75°. Transversely isotropic elastic parameters are fit based on improved existing approaches. Moreover, the strength of tested samples cut normal and parallel to foliation relevantly differ, something noted qualitatively in the past by some authors in some metamorphic anisotropic rocks. However, this difference has neither been explicitly reported for the case of other foliated sedimentary rocks such as shales, nor formalized in theoretical strength approaches. The triaxial compression experimental data on slates were fit with the Jaeger's plane of weakness (JPW) model. Strength criteria differentiating the strength in directions normal and parallel to foliation are proposed to adapt the JPW model to the observations in slate strength behavior. Other model improvement is proposed, the use of a non-linear strength criterion for the intact rock (Hoek-Brown), which shows to better represent observed strength laboratory results.

1. Introduction

When characterizing the mechanical behavior of rocks, these natural materials are often treated as linear elastic and isotropic. While this can be acceptable for a number of rocks, the occurrence of weakness planes associated to the genesis of some sedimentary and metamorphic rocks recommends accounting for anisotropy when characterizing these materials. In this way, rocks showing bedding or foliation tend to be significantly anisotropic, since they show a consistent variation of the rock properties according to the direction in which they are measured. The isotropic mechanical behavior of intact rocks has been widely studied and it is today reasonably easy to test and interpret. Nevertheless, predicting and modeling the deformability and strength of anisotropic rocks is still an insufficiently understood rock mechanics problem.¹

In recent years, a good number of studies have been carried out in

order to gain a better knowledge of the anisotropic behavior of some rocks, and particularly of shale, due to its economic importance for the shale gas and oil industries. A good knowledge of anisotropic parameters of these materials is very important since the practice of resorting to isotropic deformability parameters and failure criteria to model anisotropic rocks may produce relevant errors when predicting their strength. As pointed out by Ambrose² and also shown in this study, the strength of anisotropic rocks could attain values up to ten times and even more lower than its maximum strength, according to the direction of application of stress in relation to the orientation of the weakness planes.

Slate is a fine-grained, foliated, homogeneous metamorphic rock derived from an original shale-type sedimentary rock typically composed of clay through low-grade regional metamorphism. It is typically composed of white micas, chlorite, quartz and other minerals in a lesser amount, and the grain size is typically under 75 μm. Slate is the finest grained foliated metamorphic rock and its foliation or slaty

* Corresponding author.

E-mail address: alejano@uvigo.es (L.R. Alejano).<https://doi.org/10.1016/j.ijmms.2021.104923>

Received 4 June 2021; Received in revised form 16 September 2021; Accepted 29 September 2021

Available online 6 October 2021

1365-1609/© 2021 The Authors.

Published by Elsevier Ltd.

This is an open access article under the CC BY-NC-ND license

[\(http://creativecommons.org/licenses/by-nc-nd/4.0/\)](http://creativecommons.org/licenses/by-nc-nd/4.0/).

cleavage does not typically correspond to the original sedimentary layering, but instead it is orientated in planes perpendicular to the direction of metamorphic compression.⁴

The slates, like other metamorphic rocks, present a high degree of anisotropy caused by the processes of rock formation. These rocks form recrystallizing under oriented high stress levels, which produce the occurrence of very persistent and narrowly spaced weakness planes, the so-called cleavage, which controls the behavior and fracture patterns of these materials.^{5,6} Slates, and particularly the so-called roofing slates used to produce roof tiles, show a large degree of fissility, an ability or ease to split along flat planes, which makes them suitable for producing tiles, traditionally used to build roofs.^{3,7}

Similar anisotropic sedimentary rocks such as shales also show a large degree of anisotropy,^{8,9} but the overall stress-strain behavior shown by these materials seems to differ in some way to that of the slates. We attribute this difference to the usually weaker behavior of the forming material (clays instead of quartz and micas) and to the fact that the foliation in shales is associated to bedding planes, instead of to cleavage. Other metamorphic rocks like schists also show significant anisotropy,¹⁰ but their higher mica content makes them behave differently from slates, particularly in terms of lower frictional strength of the intact material and higher ductility.

This anisotropy of slates definitely marks the mechanical behavior of these rocks in different ways. It does produce important variations in the deformability and strength of this rock as observed by Amadei¹¹ at laboratory and field scale, as well as it controls the fracture patterns taking place when testing these rocks.⁵ From a practical engineering scope, anisotropy significantly affects the development of excavations in underground tunnel construction¹² and underground mining¹³; drill performance in TBM (Tunnel Boring Machine) and well stability^{14,15} and causes important deviations in borehole drilling.¹⁶ This anisotropy also tends to cause a great impact when interpreting in situ stress measurements.^{11,17,18} With the aim of advancing toward the solution of these problems, it is important to better understand both the elastic and strength behavior of these anisotropic rocks.

Starting from available approaches, this study focuses a rigorous characterization of the anisotropic stress-strain behavior of slates, one of the less studied anisotropic rocks. It is based in a good number of sound velocity measurements and uniaxial and triaxial stress-strain tests at different confinement levels and with different orientation of the cleavage planes. The characterization of the transversely isotropic elastic parameters is carried out based on available techniques and updated optimization approaches. Moreover, based on existing strength approaches, the authors have analyzed different possibilities of extending JPW (Jaeger's plane of weakness) strength approach considering different strength in directions parallel and normal to foliation and tentatively analyzing failure criteria different than Mohr-Coulomb for the intact rock.

The characterization of slates presented in this document was primarily devised to be used for understanding and modelling of compressive, hydro-frac^{19,20} and crack propagation tests to compute its fracture toughness.²¹ So the ultimate reason behind the presented characterization is having available reliable parameters needed to understand and model some of these tests in line with previous studies by the authors.²²

2. Deformability and strength models for foliated rocks

In this section, some available constitutive models for foliated rocks are recalled, which will be used in the forward characterization of the

stress-strain tests on slate samples. First, the transversely isotropic deformability models are introduced, as proposed by Amadei and other researchers.^{11,23–25} After that, typical anisotropic strength models are presented, based on the so-called Jaeger's Plane of Weakness (JPW)^{2,15,26} model, with potential modifications.

2.1. Constitutive model for transversely isotropic elastic rock

To completely define the fully anisotropic elastic behavior, 21 independent constants are needed in the absence of any symmetry. For this general case, Lekhnitskii²⁷ proposed to resort to the Generalized Hooke's Law for anisotropic materials. This law allows simplifications for symmetric materials, which eases computing the independent elastic constants, assuming symmetry criteria.

Different symmetry criteria produce different anisotropic responses. A transversely isotropic material shows physical properties that are symmetric about an axis normal to a plane of isotropy that can be identified as the cleavage plane for the case of slates. In this plane of isotropy, also known as transverse plane, the material properties are the same in all directions within this plane. Barla²³ developed approaches to derive elastic parameters from stress-strain tests in oriented cores for anisotropic and transversely isotropic rocks. Amadei,²⁴ building on previous studies,^{28,29} proposed the equations to calculate the independent elastic constants for four different cases of elastic symmetry, including the transversely isotropic one, in which case and due to the existing symmetry, the elastic parameters are reduced to five independent elastic constants including two elastic moduli parallel (E) and normal (E') to the foliation or isotropy plane, the two corresponding Poisson's ratios (ν and ν') and the shear modulus in the plane normal to the plane of transverse isotropy (G').

Several authors performed various studies to optimize the number and orientation of tested rock specimens to obtain the five transversely isotropic elastic parameters. Amadei,¹¹ Barla,²³ Chen et al.,³⁰ Talesnick and Bloch-Friedman,³¹ Cho et al.²⁶ and Worotnicki³² presented different approaches to obtain the values of the five independent elastic constants of various transversely isotropic rocks, using at least three different cylindrical samples with different anisotropy angles. Nejati et al.³³ introduced a method to compute the elastic constants of a transversely isotropic rock from a single uniaxial compression test, even if this type of approaches disregards the natural heterogeneity and variability of rock behavior.

Having available a good estimate of elastic anisotropic parameters is relevant for tunnel and mine stability as well for oil and gas well stability calculations, since elastic anisotropy could induce higher stress concentrations than isotropic approaches, masking in a non-conservative manner the actual excavation response.¹⁵

To orientate a transversely isotropic elastic model, it is convenient to define a local (x', y', z') and a global (x, y, z) coordinate system, as shown in Fig. 1. The local coordinate system is closely related to the foliation or isotropic plane of the rock, so its y' axis is taken as the rotation symmetry axis normal to the isotropic plane, meanwhile the x' and z' axis are contained in the isotropic plane, and the z axis and z' axis coincide.²⁶

The anisotropy angle β considered here is that formed by the foliation and the horizontal global axis x (Fig. 1). In other words, the local coordinate system can be obtained by rotating in a clockwise direction β degrees the global coordinate system around the z axis. Regarding triaxial compression tests, this angle coincides with the angle β often used to refer to the angle occurring between the vector normal to foliation planes and the direction of load of the major principal stress (σ_1) for defining the JPW strength approach.³⁴ Remark that some other

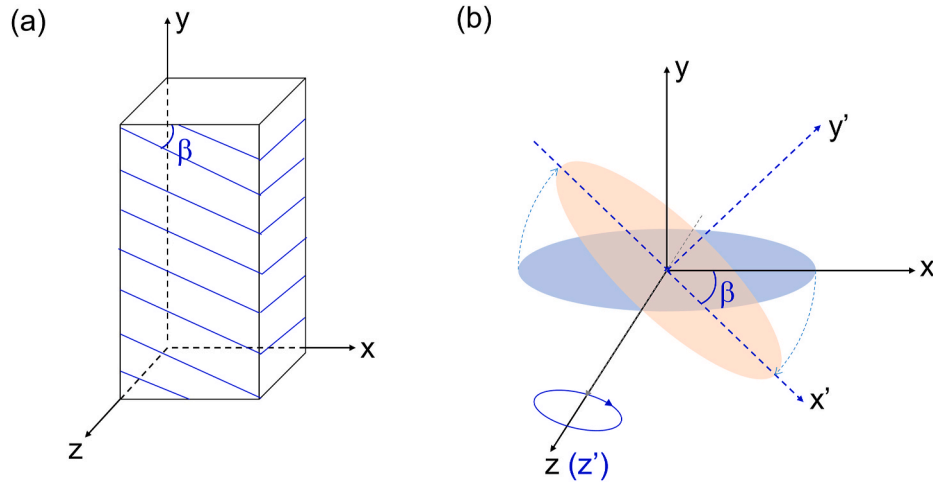


Fig. 1. a) Definition of anisotropy angle β , and b) Local (x' , y' , z') and Global (x , y , z) coordinate systems.

researchers define the angle β as that occurring between the normal to foliation and the vertical axis, so one should always be aware of the adopted convention.

The generalized Hooke's Law can be used to describe the elastic constitutive relationship of transversely isotropic rock,^{25,27} as in Equation (1). ε' , σ' and S' represent the strain (ordered collection of the 2nd order strain tensor components), the stress (same as for strain) and the elastic compliance matrix, in the local coordinate system, respectively.

$$\varepsilon' = S' \sigma' \quad (1)$$

where $\varepsilon' = [\varepsilon'_x, \varepsilon'_y, \varepsilon'_z, \gamma'_{yz}, \gamma'_{zx}, \gamma'_{xy}]^T$, $\sigma' = [\sigma'_x, \sigma'_y, \sigma'_z, \tau'_{yz}, \tau'_{zx}, \tau'_{xy}]^T$, where ε and γ refer to normal and shear strains and σ and τ refer to normal and shear stresses in the corresponding orientations and

$$S' = \begin{bmatrix} 1/E & -\nu'/E & -\nu'/E & 0 & 0 & 0 \\ -\nu'/E & 1/E & -\nu'/E & 0 & 0 & 0 \\ -\nu'/E & -\nu'/E & 1/E & 0 & 0 & 0 \\ 0 & 0 & 0 & 1/G & 0 & 0 \\ 0 & 0 & 0 & 0 & 2(1+\nu)/E & 0 \\ 0 & 0 & 0 & 0 & 0 & 1/G \end{bmatrix}$$

The above mentioned five independent transversely anisotropic elastic parameters appear in the compliance matrix S' . Additionally, for such rocks, the shear modulus G' can be expressed in terms of E , E' , ν and ν' , using the Saint-Venant's empirical solution,³⁵ as shown in Equation (2) to obtain G'_{sv} :

$$\frac{1}{G'_{sv}} = \frac{1}{E} + \frac{1}{E'} + 2\frac{\nu'}{E} \quad (2)$$

Amadei¹¹ and Worotnicki³² concluded that most of the published experimental data support the validity of the Saint-Venant approach, with some exceptions. Instead, other researchers^{26,36} found that the

Saint-Venant's solution did not agree well with the experimental data. A comparison of shear modulus between Saint-Venant approximation (G'_{sv}) and experimental data (G') of slate will be carried out in section 4 of this study.

Similar to Equation (1), in the global coordinate system, the generalized Hooke's Law can be expressed as shown in Equation (3). ε , σ and S are the strain (ordered collection of the 2nd order strain tensor components), the stress (same as for strain) and the elastic compliance matrix, in the global coordinate system, respectively.

$$\varepsilon = S\sigma \quad (3)$$

where $\varepsilon = [\varepsilon_x, \varepsilon_y, \varepsilon_z, \gamma_{yz}, \gamma_{zx}, \gamma_{xy}]^T$, $\sigma = [\sigma_x, \sigma_y, \sigma_z, \tau_{yz}, \tau_{zx}, \tau_{xy}]^T$,

$$\text{and } S = \begin{bmatrix} S_{11} & S_{12} & S_{13} & S_{14} & S_{15} & S_{16} \\ S_{21} & S_{22} & S_{23} & S_{24} & S_{25} & S_{26} \\ S_{31} & S_{32} & S_{33} & S_{34} & S_{35} & S_{36} \\ S_{41} & S_{42} & S_{43} & S_{44} & S_{45} & S_{46} \\ S_{51} & S_{52} & S_{53} & S_{54} & S_{55} & S_{56} \\ S_{61} & S_{62} & S_{63} & S_{64} & S_{65} & S_{66} \end{bmatrix}$$

All components S_{ij} of the compliance matrix S in Equation (3) can be determined by using S' and transformation matrices.^{25,27} However, for the sake of clarity, only the three components utilized in this article are presented here, as shown in Equations (4)–(6). More detailed expressions of the compliance matrices can be found in the references by Amadei,¹¹ Cho et al.,²⁶ Hakala et al.,¹⁸ or Lekhnitskii.²⁷

$$S_{12} = \frac{\sin^2 2\beta}{4} \left(\frac{1}{E} + \frac{1}{E'} - \frac{1}{G'} \right) - \frac{\nu'}{E'} (\cos^4 \beta + \sin^4 \beta) \quad (4)$$

$$S_{22} = \frac{\sin^4 \beta}{E} + \frac{\cos^4 \beta}{E'} + \frac{\sin^2 2\beta}{4} \left(-\frac{2\nu'}{E'} + \frac{1}{G'} \right) \quad (5)$$

$$S_{32} = -\sin^2 \beta \frac{\nu'}{E} - \cos^2 \beta \frac{\nu'}{E'} \quad (6)$$

Remark that the original equations by Amadei¹¹ or Cho et al.²⁶ refer to θ instead of β , as in this study. Both these angles refer to the same value, the angle formed by the foliation and the horizontal global axis x (Fig. 1).

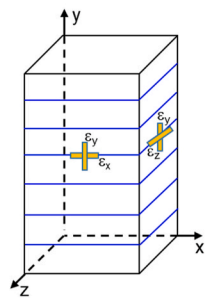
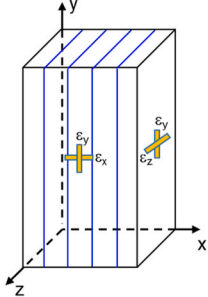
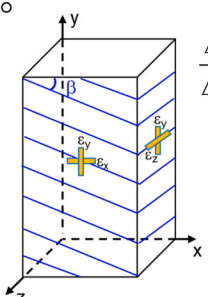
β (°)	Specimen	Equations
$\beta = 0^\circ$		$\frac{\Delta \varepsilon_x}{\Delta \sigma_y} = \frac{\Delta \varepsilon_z}{\Delta \sigma_y} = -\frac{\nu'}{E'} \quad (7)$ $\frac{\Delta \varepsilon_y}{\Delta \sigma_y} = \frac{1}{E'} \quad (8)$
$\beta = 90^\circ$		$\frac{\Delta \varepsilon_y}{\Delta \sigma_y} = \frac{1}{E} \quad (9)$ $\frac{\Delta \varepsilon_z}{\Delta \sigma_y} = -\frac{\nu}{E} \quad (10)$ $\frac{\Delta \varepsilon_x}{\Delta \sigma_y} = -\frac{\nu'}{E'} \quad (11)$
$0^\circ < \beta < 90^\circ$		$\frac{\Delta \varepsilon_x}{\Delta \sigma_y} = \frac{\sin^2 2\beta}{4} \left(\frac{1}{E} + \frac{1}{E'} - \frac{1}{G'} \right) - \frac{\nu'}{E'} (\cos^4 \beta + \sin^4 \beta) \quad (12)$ $\frac{\Delta \varepsilon_y}{\Delta \sigma_y} = \frac{\sin^4 \beta}{E} + \frac{\cos^4 \beta}{E'} + \frac{\sin^2 2\beta}{4} \left(-\frac{2\nu'}{E'} + \frac{1}{G'} \right) \quad (13)$ $\frac{\Delta \varepsilon_z}{\Delta \sigma_y} = -\sin^2 \beta \frac{\nu}{E} - \cos^2 \beta \frac{\nu'}{E'} \quad (14)$

Fig. 2. Three differently oriented specimens and corresponding equations of a transversely isotropic rock tested in uniaxial and triaxial compression with different anisotropy angles β .

Fig. 2 illustrates a classic approach to determine the five independent elastic parameters (E , E' , ν , ν' and G'). This approach is developed based on the work of Amadei,¹¹ Hakala et al.,¹⁸ Barla,²³ Cheng et al.,³⁰ Taleznick and Bloch-Friedman,³¹ Cho et al.,²⁶ Worotnicki³² and Alsuwaidi et al.³⁷ Note that Equations (7)-(14) in Fig. 2 can be derived from Equation (3).

For an initial estimate and based on the results of a specimen with $\beta = 0^\circ$, E' and ν' can be obtained through Equations (7) and (8); meanwhile, by using results from a specimen with $\beta = 90^\circ$, E and ν can be obtained through Equations (9) and (10). Then, Equation (13) can be adopted to calculate the values of shear modulus G' . This approach can provide initial estimative values of elastic constants. However, in the process of evaluating these initial values, the experimental data of ε_x from the specimen with $\beta = 90^\circ$, and ε_x , ε_z from the specimen with $0^\circ < \beta < 90^\circ$ have not been used. Thus, in the next step, the iteration of the Generalized Reduced Gradient (GRG) non-linear algorithm³⁸ will be resorted to in this study and will be run for all available experimental data, to assess in more rigorous manner the values of all elastic constants, as described in section 4.2.

2.2. Anisotropic strength

In the early 1960s, several authors carried out seminal studies on the strength of anisotropic rocks. The presence of planar anisotropy

elements such as foliation or bedding was observed to produce highly significant strength changes according to the anisotropy angle of the rock. Jaeger³⁹ suggested a theoretical application of the Mohr-Coulomb shear failure criterion, leading this proposal to a new failure criterion: the so called Jaeger's Plane of Weakness (JPW). This was based on assuming a Mohr-Coulomb failure criterion with different parameters for weakness planes and the intact rock respectively. This criterion seems to be one of the most widely used strength criteria for transversely isotropic rocks.^{2,15,26}

Walsh & Brace⁴⁰ assumed that weakness planes represent oriented Griffith cracks, so the anisotropic body was supposed to be composed of long orientated cracks embedded in an isotropic body containing an array of randomly distributed smaller cracks. Even if it was possible to account for different intact rock strengths for loading parallel and normal to weakness planes, when applying their criterion to actual slate data, the authors⁴⁰ were not able to compute or explicitly present in graphs this information. Later on, and based on the assessment of different failure criteria in the framework of modelling the failure behavior of strongly anisotropic geomaterials, and particularly that of Angers schist, Deveau et al.⁴¹, in line with Ramamurthy et al.⁴² and Bagheripour et al.,⁴³ proposed using different values of strength for the cases of loading applied parallel and normal to foliation. As these authors pointed out, the cohesion and friction of rock matrix can be determined from failure stresses obtained in triaxial tests with $\beta = 90^\circ$

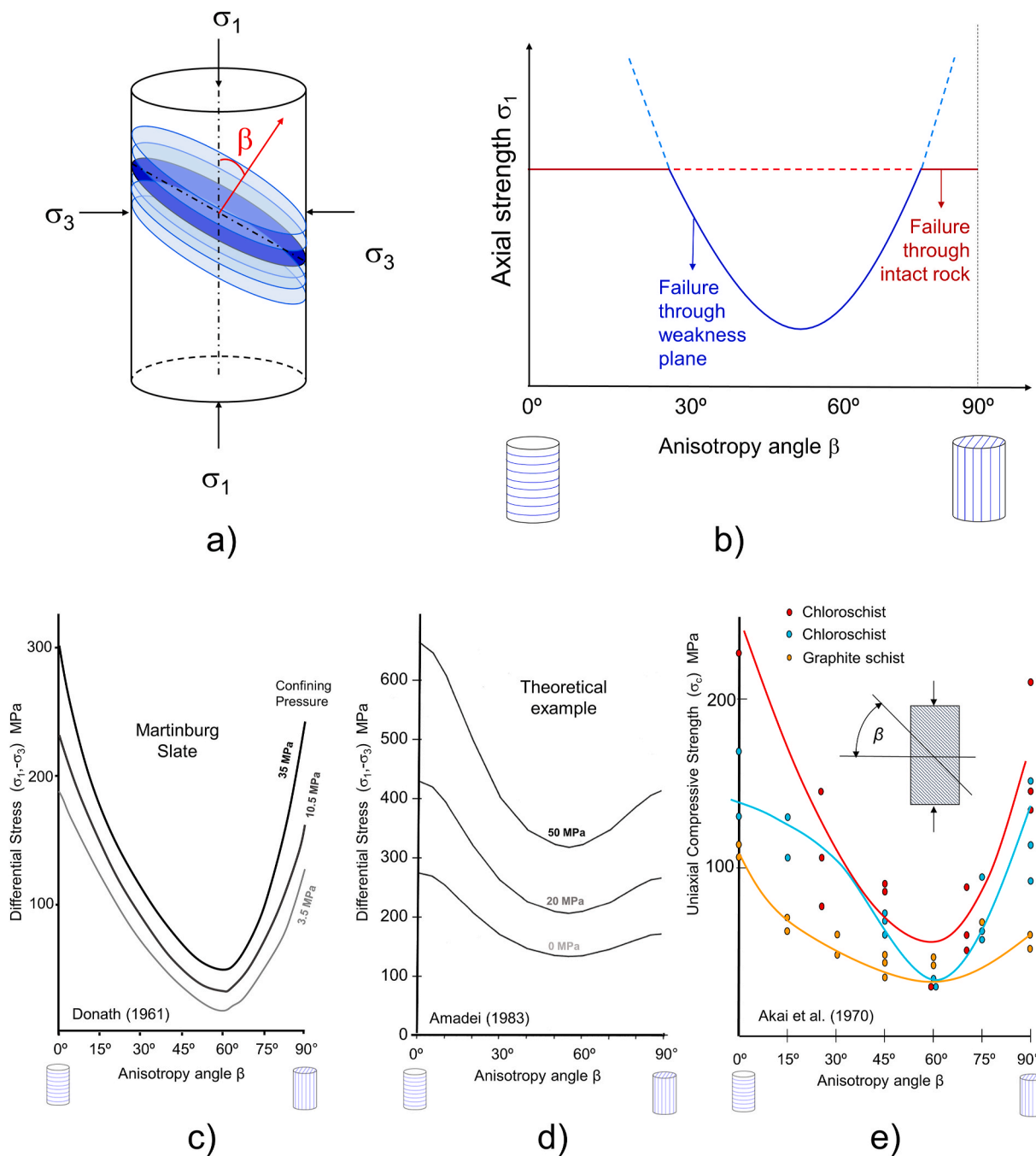


Fig. 3. In the upper part, a) Sample of a transversely isotropic material, showing the orientation of the weakness planes and b) Strength of the sample based on the Jaeger’s weakness plane (JPW) theory, showing failure associated either to intact rock strength or sliding through a weakness plane. In the lower part, representation of anisotropic strength of different materials a) Martinburg slate in triaxial strength,⁴⁷ b) Theoretical transversely isotropic strength for triaxial tests⁵⁸ and c) Different schist-type rocks in uniaxial compression.⁵⁹ Modified by the authors from the original cited sources.

and (or) $\beta = 0^\circ$, as in these orientations, the failure takes place in the rock matrix. Therefore, Deveau et al.,⁴¹ proposed different values (different fits) for $\beta = 90^\circ$ and 0° .

Hoek,⁴⁴ using a modified Griffith’s fracture criterion for anisotropic rocks, found that the propagation of cracks occurred in two different ways: in the direction of the weakness planes (primary cracks) and randomly oriented to grain boundary (secondary cracks). Pariseau⁴⁵ made a modification of the Hill’s theory of plasticity for metals⁴⁶ in the form of an extension of the Drucker-Prager criterion fulfilling the symmetry requirements for the transversely isotropic materials. The model allows calculation of the five transversely isotropic elastic parameters, and predict a smooth continuous variation of strength in relation to the

anisotropy angle. While this produces smoother results, the derived parameters lack physical meaning, so the JPW tends to be more widely used.

Donath^{47–49} performed different studies on anisotropic materials to obtain the influence of the anisotropy on fracture strength and failure angle in foliated rocks. Mogi and co-workers^{50,51} carried out different true triaxial studies on anisotropic rocks focusing on the effects of stress states on fracture orientations. Since Mohr theory do not consider the intermediate principal stress, a true triaxial approach can often better predict the behavior of the rock. In these studies, the deformational and strength properties of many rocks were observed to be also affected by the intermediate principal stresses. Kwaśniewski,⁵² compiled different

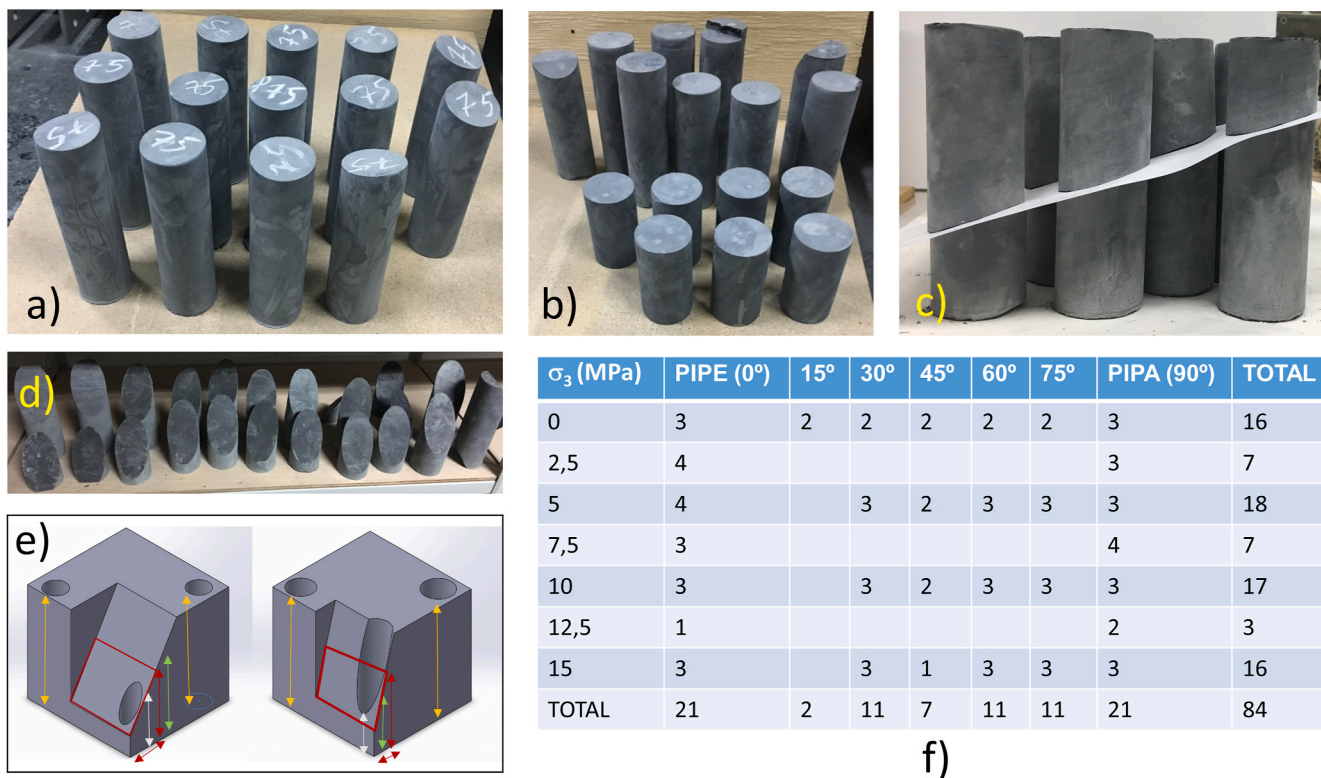


Fig. 4. Illustrations showing the difficulties in cutting samples with inclined foliation due to slate fissility: a) Cored samples with foliation inclined 75°, b) Cored samples with foliation inclined 60°, c) Cored samples with foliation inclined 15°, intercepted by a particularly weak foliation plane that makes very difficult to obtain samples of this type, d) Rejected broken material corresponding to samples with foliation inclined 60°, e) Sketch showing geometrical constraints to obtain long enough samples for highly dipping foliation, f) Table indicating the number of samples successfully prepared and tested according to foliation dip and confining stress.

works, included the mentioned above, studying the role of the intermediate stress in anisotropic rocks.

2.2.1. Typical isotropic failure criteria for rocks

Strength of rocks is modelled by means of failure criteria. The two most used failure criteria for standard isotropic rocks are the Mohr-Coulomb^{34,53,54} and the Hoek-Brown^{55,56} failure criteria.

The Mohr-Coulomb criterion proposes that failure occurs along a shear plane when the shear stress τ acting along this plane, where a normal stress σ_n is applied, reaches a critical value controlled by a cohesive force and a frictional resistance according to:

$$\tau = c_o + \sigma_n \tan \varphi_o \tag{15}$$

where c_o refers to cohesion and φ_o to friction angle of the intact rock. This failure criterion can be also expressed^{34,57} as stating that failure will occur if and when:

$$\sigma_1 = 2c_o \tan \beta_o + \sigma_3 \tan^2 \beta_o \equiv \sigma_{co} + \sigma_3 \tan^2 \beta_o \tag{16}$$

where $\sigma_1 \geq \sigma_2 \geq \sigma_3$ are the three principal stresses, σ_{co} is the uniaxial compressive strength of the intact rock according to the Mohr-Coulomb criterion and $\beta_o = 45^\circ + (\varphi_o / 2)$ is the angle between the normal vector to the newly formed failure plane and the maximum principal stress.

The Hoek-Brown failure criterion does not seek a particular shear failure plane so it is referred to the principal stresses and, for the case of intact rocks, predicts failure based in two parameters: the uniaxial compressive strength of the intact rock σ_{ci} and a frictional parameter m , according to:

$$\sigma_1 = \sigma_3 + \sqrt{m \cdot \sigma_{ci} \cdot \sigma_3 + \sigma_{ci}^2} \tag{17}$$

Note that σ_{co} and σ_{ci} represent uniaxial strength of the intact rock, so

they tend to be similar but they are not equal due to the different shape of the failure criteria considered, one linear, Mohr-Coulomb; and the other one non-linear, Hoek-Brown.

According to authors' experience and published results,⁵⁵ sedimentary rocks such as sandstone tend to fit well the Mohr-Coulomb criterion, but for harder rocks, where sometimes the definition of a shear plane is unclear, a non-linear criterion such as Hoek-Brown tends to better fit actual test results of intact hard rock samples. The Hoek-Brown failure criterion is also very popular, due to its ability to be extended to rock mass behavior, starting from intact rock strength data and rock mass classification systems.

For strongly foliated rocks, where distinct parallel weakness planes pervasively occur, the direction normal to these planes can be assumed to be a rotational symmetry axis. So planes normal to this axis have identical mechanical properties but different (weaker) than planes parallel to this axis, so anisotropic strength approaches are in order.

2.2.2. Jaeger's plane of weakness (JPW) anisotropic strength model

Jaeger³⁹ proposed a strength conceptual approach for these foliated media. Failure along these foliation or weakness planes (Fig. 3a) is assumed to be governed by a Mohr-Coulomb-type criterion, with a cohesion c_w and a friction angle φ_w of the weakness plane typically lower than those corresponding to intact rock.³⁴ This can be expressed in terms of the major principal stresses as⁵⁷:

$$\sigma_1 = \sigma_3 + \frac{2(c_w + \sigma_3 \tan \varphi_w)}{(1 - \tan \varphi_w \cot \beta) \sin 2 \beta} \tag{18}$$

where β is the angle between σ_1 and the normal to the planes of weakness. Alternatively, the following Equation can also be used:

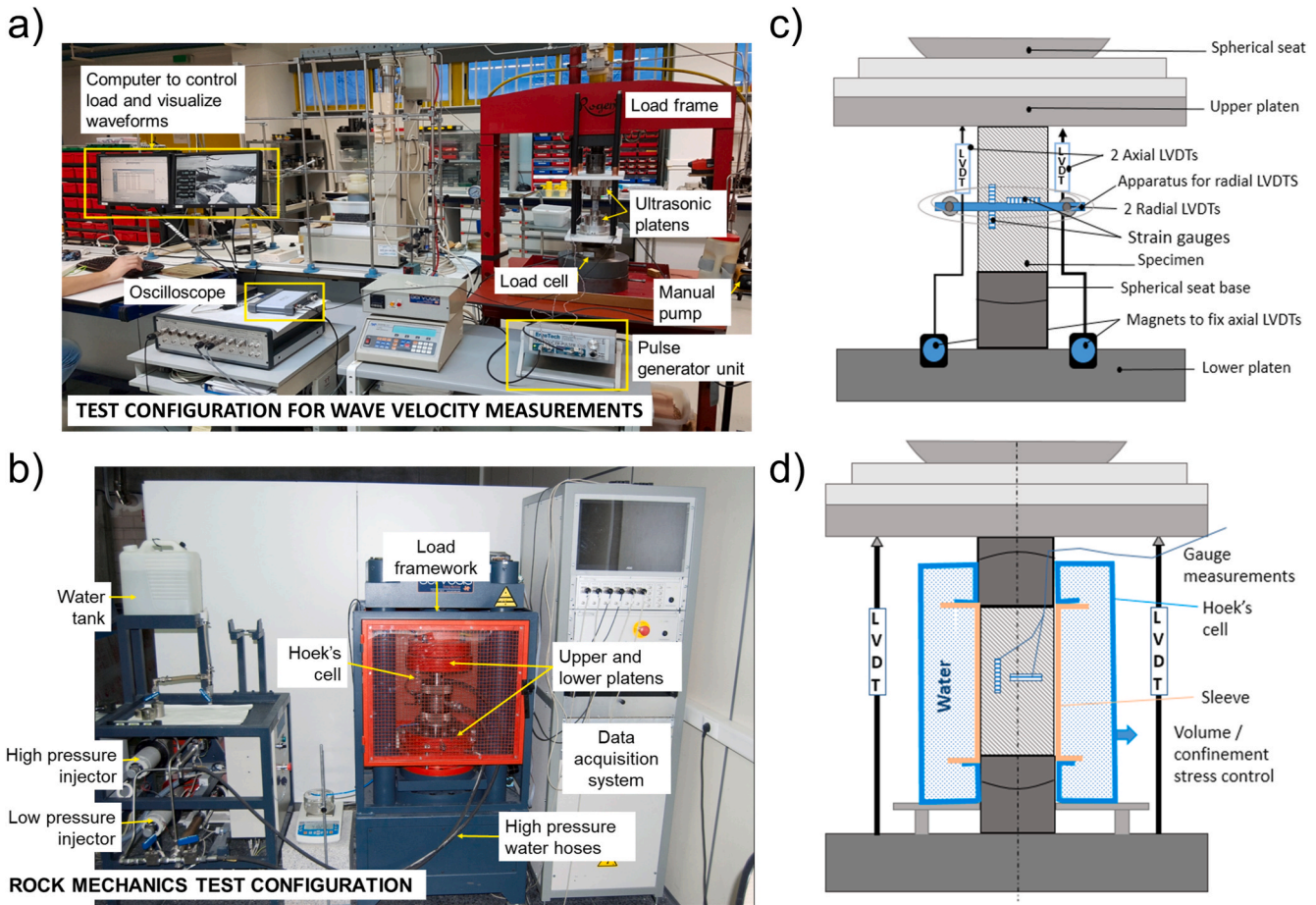


Fig. 5. Laboratory equipment: a) Set-up for wave velocity measurement at the University of La Coruña b) Loading frame for compressive rock mechanics testing at the University of Vigo, c) Set-up used for UCS testing and d) Set-up used for triaxial compressive testing.

$$\sigma_1 = \frac{2 \cdot c_w + \sigma_3 \cdot (\sin 2\beta + \tan \varphi_w - \cos 2\beta \cdot \tan \varphi_w)}{\sin 2\beta - \tan \varphi_w \cdot (1 + \cos 2\beta)} \quad (19)$$

Failure through intact rock is also possible on a different plane, whose normal vector makes an angle $\beta_o = 45^\circ + (\varphi_o/2)$ with the direction of σ_1 . If the usual Coulomb criterion (Equation (15)) is satisfied:

$$\sigma_1 = 2c_o \tan \beta_o + \sigma_3 \tan^2 \beta_o \quad (20)$$

where c_o is the cohesion of any plane other than the bedding plane, and the subscript o refers to the “intact rock”, i.e., the rock in the absence of these bedding planes.

For every fixed value of σ_3 , the value of σ_1 required to cause failure somewhere within the rock will then be equal to the smaller of the two values given by Equations (18) or (19) and (20); see Fig. 3 b. If the value given by Equation (18) or (19) is less than that given by Equation (20), failure will occur along a plane of weakness. If the value given by Equation (18) or (19) is greater than that given by Equation (20), failure will occur through a plane (shear band) passing through the “intact rock”, whose normal vector makes an angle β_o with the direction of σ_1 .⁵⁷

So, basically the concept behind Jaeger’s plane of weakness (JPW) strength criterion consists in associating two potential failure mechanisms to rock strength: one associated to intact rock that can be modelled by a Mohr-Coulomb criterion with parameters c_o and φ_o and the other associated to shear along preexisting weakness planes having a particular orientation (β) and with a Mohr-Coulomb shear criterion with parameters c_w and φ_w .

Despite the fact that the JPW model estimates an equal maximum strength for all foliation dips associated to intact rock, and notably for 0 and 90°, results compiled by different authors suggest otherwise for

some metamorphic rocks. For instance, Donath,⁴⁷ based on triaxial test results in Martinburg slate; Amadei⁵⁸ theorizing or Akai et al.,⁵⁹ for UCS tests in different types of schist illustrated how the strength in samples oriented normal to foliation ($\beta = 0^\circ$) tends to be significantly larger than those corresponding to samples oriented perpendicular to foliation ($\beta = 90^\circ$), as illustrated in Fig. 3c, 3d and 3e. To account for this difference of intact rock strength for the loading normal and parallel to foliation some authors^{41–43} have suggested a version of the JPW strength approach considering differential truncation at shoulders, that is, different levels of Mohr-Coulomb strength at the left (typically higher) and right (typically lower) sides of the strength controlled by the failure through the weakness plane.

A potential modification to the JPW approach can include substituting the Mohr-Coulomb failure criterion for intact rock for another available intact rock failure criterion such as Hoek-Brown. Other potential modifications for this JPW approach can be proposed by changing the Mohr-Coulomb shear failure criterion assumed for the weakness planes by other potential shear strength criteria suitable for weakness planes found in rocks, such as for instance those proposed by Barton,⁶⁰ Maksimovic⁶¹ or others.

3. Experimental work

With the aim of characterizing slate, sufficient material of this rock cut in 35 cm side rock blocks was acquired from a quarry site located in O Barco de Valdeorras, sited in the north-west of Spain. The chosen slate belongs to the Luarca series, where slate shows marked foliation and high consistency and presents black to very dark blue colour. This material is quarried to produce roofing slate tiles, so it presents high fissility.

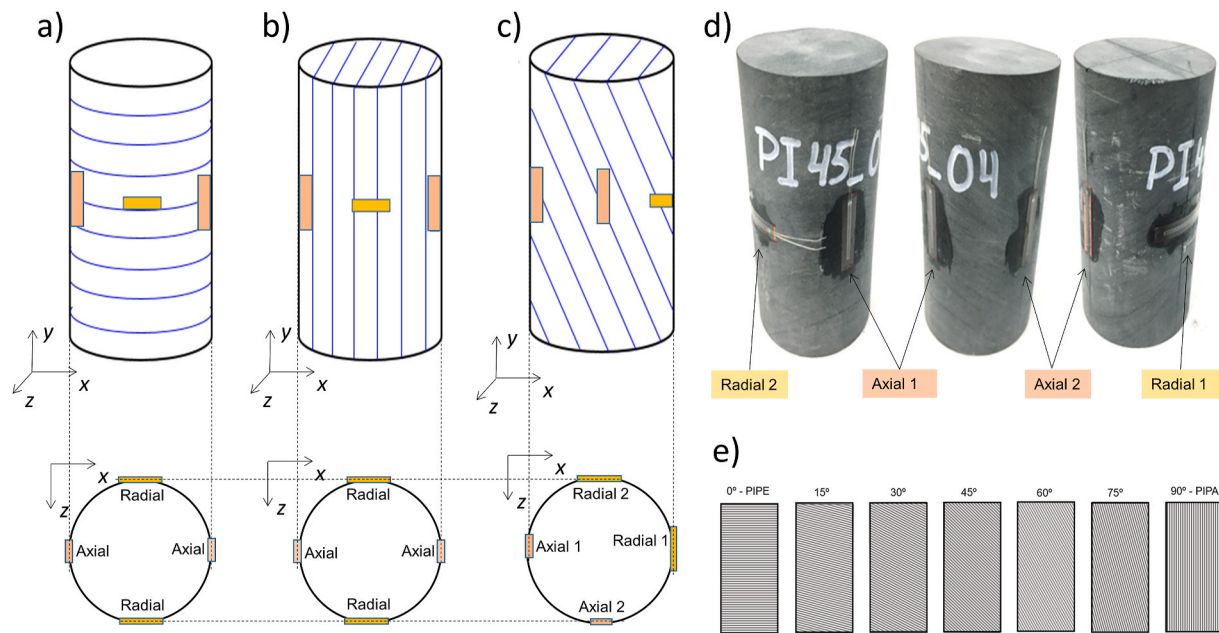


Fig. 6. Strain gauges configuration for a) PIPE ($\beta = 0^\circ$), b) PIPA ($\beta = 90^\circ$), c) PIXX ($0^\circ < \beta < 90^\circ$), d) actual sample PI45-04 with gauges glued and e) sketch of samples with foliation forming 0 (PIPE), 15, 30, 45, 60, 75 and 90° (PIPA) with the horizontal. Axial and radial represent the corresponding strain gauges.

Samples were prepared with the help of a saw disk machine (CEDIMA model CTS-265, 400 mm radius disk), a drilling machine (WEKA, model DK22) and a grinding machine.

3.1. Rock samples and specimen preparation

The experimental program was carried out in two stages. In the first stage groups of around 30 cylindrical 54 mm diameter (and at least double height) samples were cored, cut and grinded in directions perpendicular (named PIPE, $\beta = 0^\circ$) and parallel (name PIPA, $\beta = 90^\circ$) to foliation. These samples were weighed after been submersed in water for 15 days and after drying in an oven for 24 h, so dry and saturated densities and connected porosity were computed. All these samples were then submitted to non-destructive wave propagation measurements and then to uniaxial or triaxial ($\sigma_3 = 2.5, 5, 7.5, 10, 12.5$ and 15 MPa) compressive tests. In the compressive tests, only in some cases gauges were used to measure strain in the samples while testing.

In the second stage of testing the authors tried to obtain groups of around 25 cylindrical 54 mm diameter samples with foliation forming an angle β of 15, 30, 45, 60 and 75° with the horizontal (named PIXX, where XX refer to the foliation dip). This implied pre-cutting of the original block, which, due to the fissility of the rock, was not an easy task. Although possible in some cases, as for the 60 and 75° foliation cases (Fig. 4a and b), a large number of samples broke in the process of drilling, cutting and grinding (Fig. 4c and d). For the case of $\beta = 15^\circ$, only two samples were eventually obtained and for the case of $\beta = 45^\circ$ only 12, out of which 5 broke in the process of pre-loading in the press. For the 60 and 75° foliated samples a rather large quantity of material was needed to produce slender enough samples (Fig. 4e).

In all these samples corresponding to the second stage, the density parameters were tested, but only in two samples corresponding to each foliation angle, velocity of propagation was measured, something decided in the light of the rather regular values obtained for the other samples.

All these samples were mechanically tested and, for this group, duly oriented gauges were glued to all samples to compute the elastic response of these samples tested at confinements of $\sigma_3 = 0, 5, 10$, and 15 MPa. All in all, the experimental program covered eventually 84 tested samples corresponding to different foliation dips and tested at different

confinements according to the table shown in Fig. 4 f.

Based on the dry and saturated weigh of the samples, we obtained average values of connected porosity of 0.63%, average grain density 2,778 kg/m³ and average dry and saturated densities of 2,761 and 2,767 kg/m³ respectively, with standard deviations of 7 kg/m³ for around one hundred samples, indicating very constant densities.

3.2. Wave velocity testing

For wave velocity measurement, recommendations provided by ASTM,⁶² similar to ISRM,⁶³ were followed. The equipment used for the wave velocity measurements (Fig. 5a) included the pulse generator unit (with a variable pulse width range of 1–100 ns) with P-S1–S2 wave selection manually controlled; a digital oscilloscope, which digitalized the waveforms, connected to the computer where the waveforms were visualized, and the compression platens with acoustic ultrasonic emitter/receiver. The piezoelectric crystals used in the ultrasonic emitter/receiver were PZA-5A (Lead, Zirconate, Titanate) crystals with a central frequency of 1.3 MHz.

All specimens were saturated in water for at least two weeks before testing. In order to improve the contact among the transducers and the specimens and to ensure a proper transmission of waves, an appropriate coupling gel and a 1 MPa load were applied. In the process of apply this low load, two 45° foliation dip samples broke. Once installed the sample in this set-up, the oscilloscope output waveforms were visually checked, and the recorded for post-processing of P-wave, S1-wave, and S2-wave data. These graphs are then used to estimate the wave propagation velocity by means of a software that allows visualization, doing basic mathematical operations and saving of the waveforms.

3.3. Rock mechanics testing

For the compressive tests including uniaxial and triaxial strain-strength tests, a press system model MES 200 from Servosis S.L. was used (Fig. 5b). This press has a load capacity up to 2000 KN, and can be servo-controlled in different manners, in terms of strain or stress. Hoek's cells can be installed within the frame and the confinement stress can also controlled by the servo system.

The 54 mm diameter samples were tested for uniaxial (Fig. 5c) and

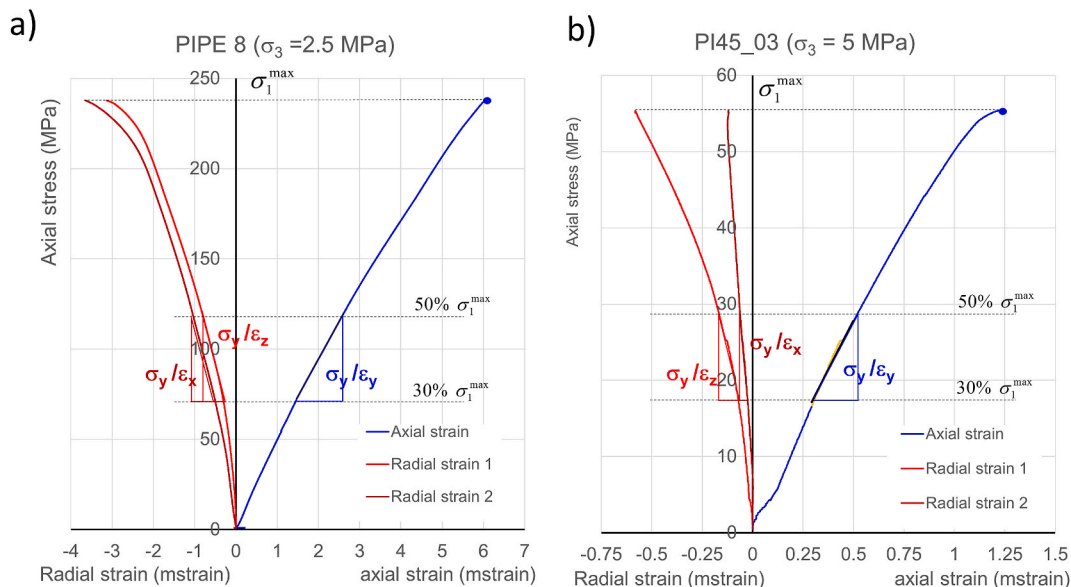


Fig. 7. Stress strain curves of two samples: a) a sample cut perpendicular to foliation and b) sample cut forming an angle of 45° with foliation, presenting axial stress versus average axial strain and two radial strain results. The peak axial strain is estimated in each case as the maximum axial stress recorded. Strain estimates are taken based on the slope of the stress-strain curves following the approach explained in the text and illustrated in Fig. 2.



Fig. 8. Photograph of representative slate samples after testing for various foliation inclinations and confinements.

triaxial (Fig. 5d) conditions including strain measurements with LVDTs in all cases and with strain gauges in some cases. In all specimens with inclined foliation (from 15 to 75° as shown in Fig. 6e), strain gauges were glued in the sample using the configuration of two strain gauges in the radial direction and two in the axial axis, separated 90° among them, and starting with an axial gauge glued in the intersection of a vertical plane containing the dip direction with the sample periphery, as it can be seen on Fig. 6c and d. In the samples named PIPA and PIPE with foliation parallel and normal to major principal stress the axial and

radial axis gauges were only used in some samples according to the sketch showed in Fig. 6a and b., that is with radial and axial gauges glued in the symmetry plane, which produced some difficulties in interpretation for the PIPE case, so the set-up was changed for the PIXX samples.

For triaxial tests, samples were installed in the Hoek's cell (Fig. 5d) and pre-loaded with a force somewhat smaller than that needed to produce the nominal confinement. Then water was injected in the Hoek's cell to achieve the needed confinement. At this point, the strain

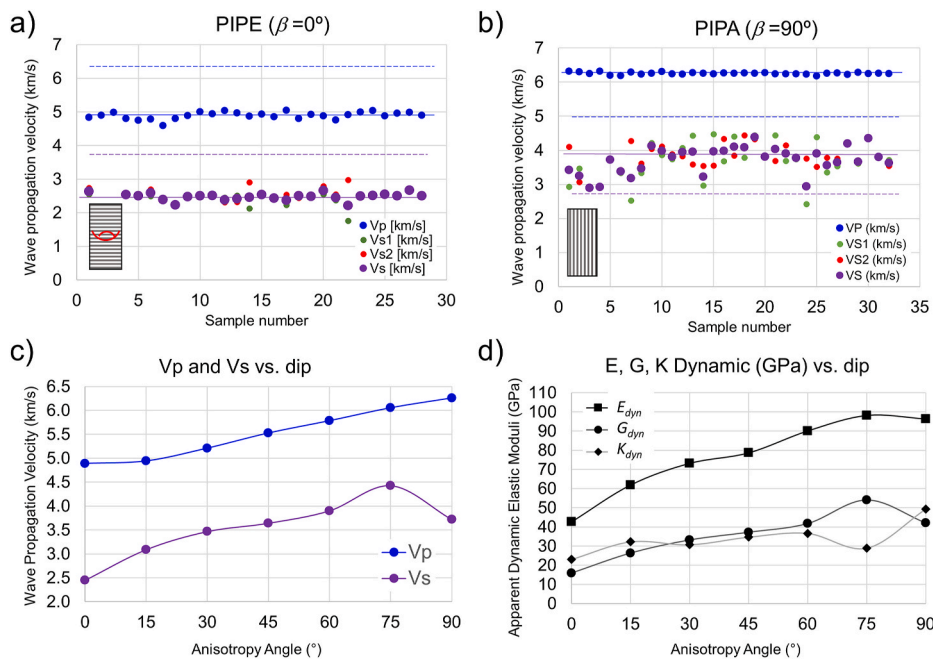


Fig. 9. Results of wave propagation velocity in slate samples. a) P- and S- wave velocities in samples cut perpendicular to foliation, b) P- and S- wave velocities in samples cut parallel to foliation, c) average P- and S-wave velocities graphed versus foliation angle and d) Dynamic elastic moduli represented in relation to foliation angle. In a) and b) S wave velocity (Vs) is averaged from velocities measured in the 2 polarization planes (VS1 and VS2) and continuous horizontal lines represent average values.

measurements were zeroed and the tests start from zero strain and the pre-loading force. Then, the sample was axially loaded in a strain controlled manner with a rather large velocity until attaining half of estimated strength. Then the test is continued with a low axial strain velocity manually controlled up to failure.

The corresponding axial stress-axial strain curves (averaging the two axial gauge measurements) and axial stress-radial strain curves (for the two available gauges) were recovered, as shown in Fig. 7 for a PIPE ($\beta = 0^\circ$) sample and a PI45 ($\beta = 45^\circ$) sample.

Peak strength values were recovered in all cases. When available, the inverse of the stress-strain slope for the average axial and the 2 radial gauges was obtained, based on the models of Fig. 2 and as depicted in the stress-strain graphs in Fig. 7. These slopes ($\Delta\sigma/\Delta\epsilon$) were computed for a range of stresses between 30 and 50% of peak strength to cover the typically elastic part of the test, though sometimes this range was adjusted. In some cases, usually due to testing problems, they were considered not reliable for further analysis. Results of peak stress and the reliable stress-strain inverse slopes ($\Delta\epsilon/\Delta\sigma$) for all the available samples and velocity measurements were compiled in Table 1 of the Appendix.

After testing, the broken samples were removed from the Hoek's cell, photographed and carefully observed. A sample of failed specimens for different foliation inclinations and confining stress levels is illustrated in Fig. 8. For the specimens with foliation dip in the range from 15 to 75°, the failure mechanism observed was typically clean sliding through a foliation plane, even if "en echelon" failure through foliation planes and newly formed (typically vertical) surfaces were occasionally observed. For the samples cut perpendicular to foliation (PIPE or $\beta = 0^\circ$), double cone failure, as in typical isotropic rocks, was sometimes observed, but also newly formed shear bands, more common for unconfined tested samples. Finally, for samples cut parallel to foliation (PIPA or $\beta = 90^\circ$), failure through axial splitting vertical foliation planes was observed, where often, rock lamella or plates (thin rock pieces between foliation planes) bent producing a buckling failure mechanism. Sometimes, shear bands also formed in these cases.

4. Results and interpretation

In this section we present, interpret and briefly analyze results of the tests carried out on slate samples including wave propagation and stress-

Table 1

Average results of wave propagation velocities and dynamic elastic parameters.

	Anisotropy Angle ($^\circ$)	VP (km/s)	VS (km/s)	E dyn (GPa)	ν dyn (-)	G dyn (GPa)	K dyn (GPa)
PIPE	0	4.89	2.45	42.68	0.34	15.95	23.08
PI15	15	4.94	3.09	61.91	0.18	26.37	32.23
PI30	30	5.21	3.47	73.18	0.11	33.2	30.71
PI45	45	5.53	3.64	78.67	0.08	37.21	34.67
PI60	60	5.78	3.90	90.09	0.09	41.75	36.62
PI75	75	6.06	4.43	98.16	0.00	54.03	28.94
PIPA	90	6.26	3.72	96.38	0.16	42.1	49.24

strain tests. Interpretation of rock mechanics tests addresses deformability and strength separately.

4.1. Wave velocity results

The equipment described in section 3.2 records the P and S waveforms, in particular stacked versions of 32 of these waves, in every case. With the obtained waveforms, picking of first arrival time of the waves is carried out based on an R code implementing the Akaike Information Criterion (AIC),⁶⁴ which was chosen due to its history of reliable results.⁶⁵ This R-code followed previous studies by the authors and standards.^{62,66}

Initially, all the samples with foliation perpendicular (PIPE, $\beta = 0^\circ$) and parallel (PIPA, $\beta = 90^\circ$) were tested, including some not mechanically tested. Results of P and S wave propagation velocities in these samples are graphed in Fig. 9a and b. P-wave velocity results were easier to pick and very regular, S-wave velocity results were more difficult to correctly pick and more variation was observed, particularly for the samples cut parallel to foliation. The values obtained for P and S wave velocities in these cases, are in accordance with the values reported by Rodríguez Sastre et al.⁶⁷ in similar slates.

For the samples cut forming and inclined angle with foliation ($\beta = 15, 30, 45, 60$ and 75°) only two specimens were tested for every case. The synthesized average results of all the tests are presented in Table 1 and graphed against foliation dip in Fig. 9c. The propagation velocity of P waves tends logically to increase with growing dip of the foliation angle, due to the potential of the weakness plane to reflect waves. The

Table 2
Results of elastic parameters.

	E (GPa)	E' (GPa)	E/E'	ν (-)	ν' (-)	ν/ν'	G' (GPa)	G'_{sv} (GPa)	$[G' - G'_{sv}]/G'$
Initial	75.51	38.44	1.79	0.24	0.33	0.83	19.52	17.79	7.6%
Final	68.22	38.04	1.96	0.23	0.28	0.72	19.45	17.97	8.9%

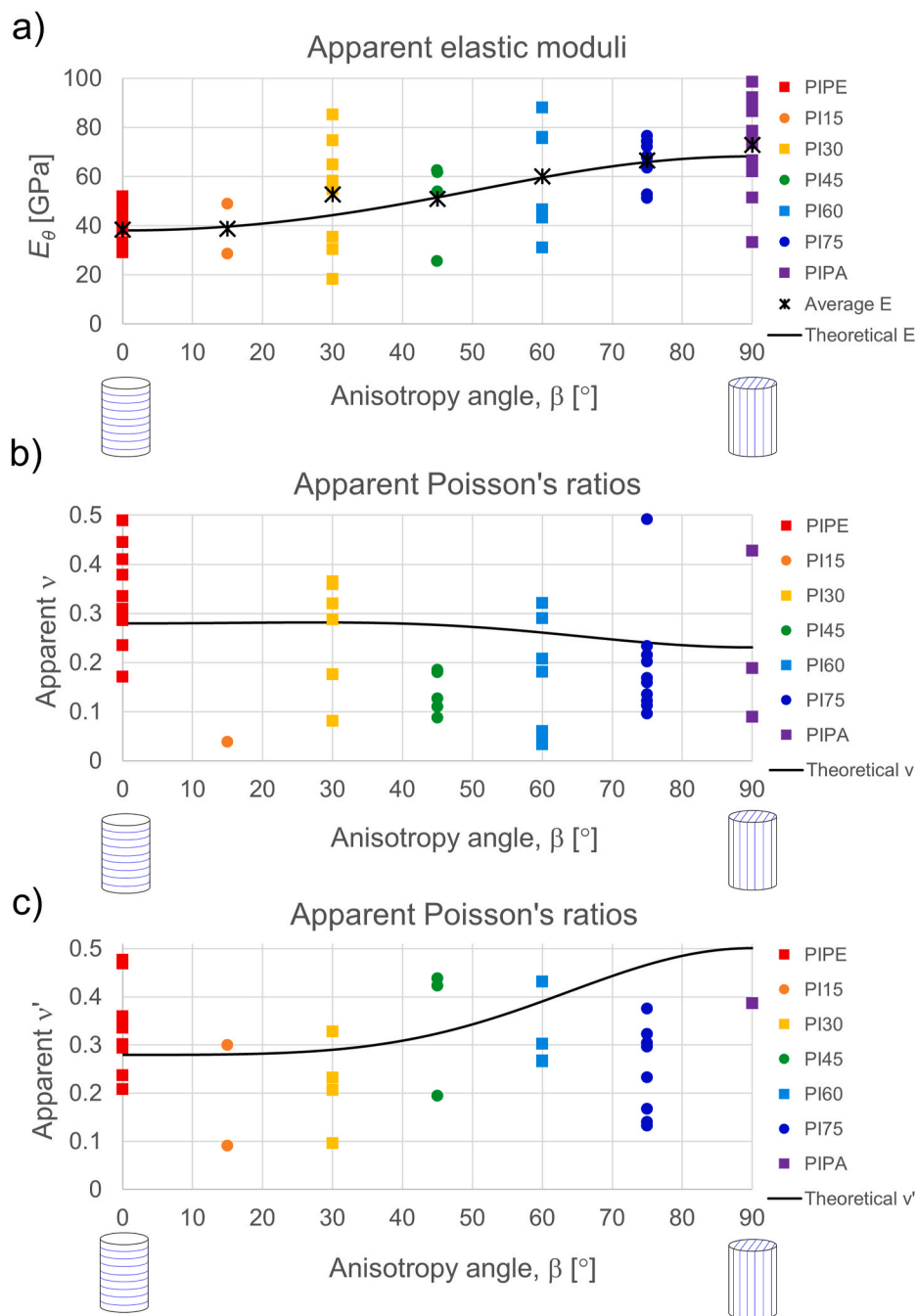


Fig. 10. Graph representing a) apparent elastic moduli, b) apparent Poisson’s ratio ν , and c) apparent Poisson’s ratio ν' , versus anisotropy angle of all tests (colored dots), average empirical values (stars) and theoretical approach (black line).

apparent dynamic parameters derived from these velocities based in classical formulations⁶² are also computed, presented in Table 1 and graphed against foliation angle in Fig. 9 d. The dynamic elastic modulus anisotropic ratio, E/E' is slightly over 2, denoting a highly anisotropic material, in line with values reported by Worotnicki³² for similar rocks.

4.2. Anisotropic characterization of rock deformability

4.2.1. Deformability

The five elastic constants (E , E' , ν , ν' and G') for a transversely isotropic rock are listed in Table 2. These constants were calculated from the gauges measurements obtained from the 67 tests with gauge results

presented in Table 1 in the Appendix. Both, initial estimates and final fine-tuned values of elastic parameters are presented in Table 2.

The initial values of elastic constants are calculated based on the approach shown in Fig. 2, while the final values were evaluated by using the Generalized Reduce Gradient non-linear algorithm (the so-called GRG method)³⁸ based on the initial values and all experimental data. Note that part of the data has not been used in the approach of obtaining the initial values, instead, all experimental data are used in determining the final values, as described in section 2.1. To this end, the final values could better represent experimental data, compared with those initial values.

It can be seen from Table 2 that the anisotropic ratio of elastic moduli (E/E') is 1.96. This value is close to 2, in line with dynamic results, and it corresponds to a high anisotropic material. Additionally, in order to investigate the validity of Saint-Venant's empirical solution for shear modulus, this empirical estimate (G'_{sv} , see Equation (2)) is compared with the computed values (G'), showing 8.9% prediction error.

The main idea of the GRG method is to solve the nonlinear problem dealing with active inequalities, and the variables are separated into a set of dependent variables and independent variables.³⁸ Then, the reduced gradient is computed in order to find the minimum of a control function in the search direction.³⁸ This process is repeated until the convergence is obtained.³⁸ In this study, the authors sought for a control function able to be representative of the elastic deformational response of the specimen. After various trials with different functions, the first strain invariant (J_1) shows to be a reasonably representative function providing consistent results, so it was chosen as a suitable control function of elastic parameters:

$$J_1 = \varepsilon_x + \varepsilon_y + \varepsilon_z = \varepsilon_I + \varepsilon_{II} + \varepsilon_{III} \quad (21)$$

where ε_x , ε_y and ε_z represent the strains from the gauges measurements in the x, y and z directions, respectively; ε_I , ε_{II} and ε_{III} are the theoretical solutions of strains in the x, y and z directions, respectively. The difference of the first strain invariant between experimental results (see Appendix) and theoretical solutions (see Fig. 2), Δ , is set as the objective function, as shown in Equation (22). Δ varies depending on the elastic constants.

$$\Delta = \left(\frac{\Delta \varepsilon_x}{\Delta \sigma_y} + \frac{\Delta \varepsilon_y}{\Delta \sigma_y} + \frac{\Delta \varepsilon_z}{\Delta \sigma_y} \right) - \left(\frac{\Delta \varepsilon_I}{\Delta \sigma_y} + \frac{\Delta \varepsilon_{II}}{\Delta \sigma_y} + \frac{\Delta \varepsilon_{III}}{\Delta \sigma_y} \right) \quad (22)$$

In this example, the Young's Moduli are constrained from 1 to 100 GPa, the Poisson's ratios are constrained from 0.01 to 0.5, and the shear moduli are constrained from 1 to 50 GPa. Then, the iteration of the algorithm is carried out, which varies the parameters E , E' , ν , ν' and G' , to obtain the optional (final) elastic constants where $\sum \Delta$ is closest to 0. The GRG algorithm is set to stop when Δ is minimized for the predefined range of inputs. It finally outputs the final values of elastic constants shown in Table 2.

4.2.2. Apparent elastic moduli

The apparent Young's moduli (E_θ) is the observed stiffness response of the sample (σ_y/ε_y) and can be theoretically computed as $1/S_{22}$ in Equation (13). Apparent elastic moduli versus the anisotropy angle β , are represented in Fig. 10 a, obtained from the laboratory tests (colored dots and stars) and the theoretical solutions (black line).

As it can be observed in Fig. 10 a, the average values of elastic moduli show the lowest value at $\beta = 0^\circ$ and the highest value at $\beta = 90^\circ$, with an approximate ratio of E/E' is 1.89. The apparent Young's modulus at $\beta = 0^\circ$ (E') ranged from 29.1 GPa to 51.9 GPa, whereas a larger scatter is observed for Young's modulus at $\beta = 90^\circ$ (E). A visual comparison of theoretical results and experimental data, confirms that the theoretical curve tends to lie in the middle of experimental data. Both results match well and have a similar S-shape trend, which suggest that the transversely isotropic elastic model is a reasonably accurate constitutive modelling approach for the deformability of slates.

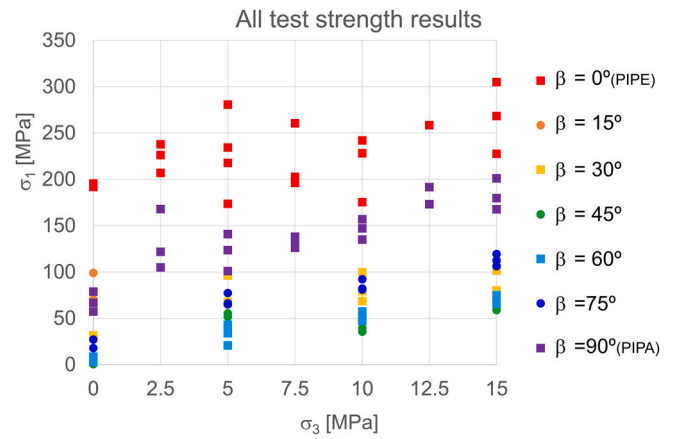


Fig. 11. Data results of all strength tests on major – minor principal stress axes. A color code is given in the legend to differentiate anisotropy orientations. (For interpretation of the references to color in this figure legend, the reader is referred to the Web version of this article.)

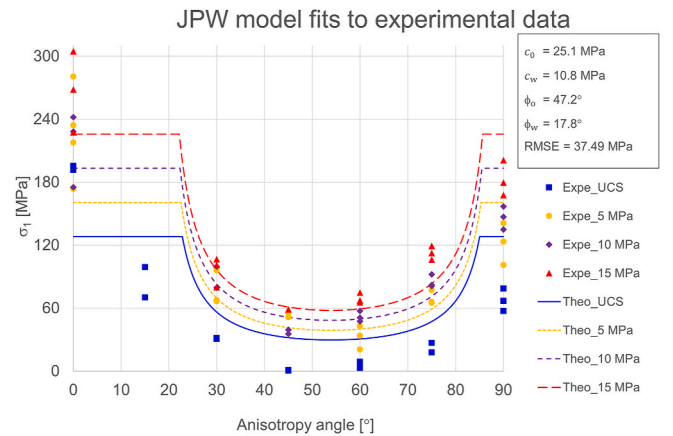


Fig. 12. JPW model fits to experimental data. 'Expe' and 'Theo' in the figure represent experimental data and theoretical solutions, respectively.

4.2.3. Apparent Poisson's ratios

Poisson's ratios for slate samples can be calculated from the axial and radial strain gauge measurements in uniaxial and triaxial compression tests. The apparent Poisson's ratios ν and ν' are shown in Fig. 10b and 10c, respectively. Interpretation of apparent ν and ν' for slate test results is not an easy task, for these values tend to show a large scatter in experimental data. This scatter, generally observed in isotropic elastic rocks,⁶⁶ is apparently more marked for the case of transversely isotropic natural materials.^{2,18,68}

According to theoretical transversely isotropic theory, both apparent ν and ν' must show the same value for PIPE samples ($\beta = 0^\circ$), while ν' should be larger than ν for PIPA samples ($\beta = 90^\circ$). This seems to be also the case for experimental results, since for PIPE samples, strains in the x direction (ε_x) are the same as the ones in the z direction (ε_z), while for PIPA samples, ε_x is observed to be larger than the corresponding ε_z . Interestingly, the values of apparent ν' attain levels slightly over 0.5, something that can also be observed for other highly anisotropic rocks. According to elastic parameters provided by Cho et al.,²⁶ Yeoncheon schist would show values of apparent ν' over 0.5 for PIPA.

4.3. Strength anisotropy

Table Appendix 1 compiles the peak strength values observed for all 84 specimens successfully tested in the laboratory. Fig. 11 illustrates that the minimum strength is observed for foliation angles in the range

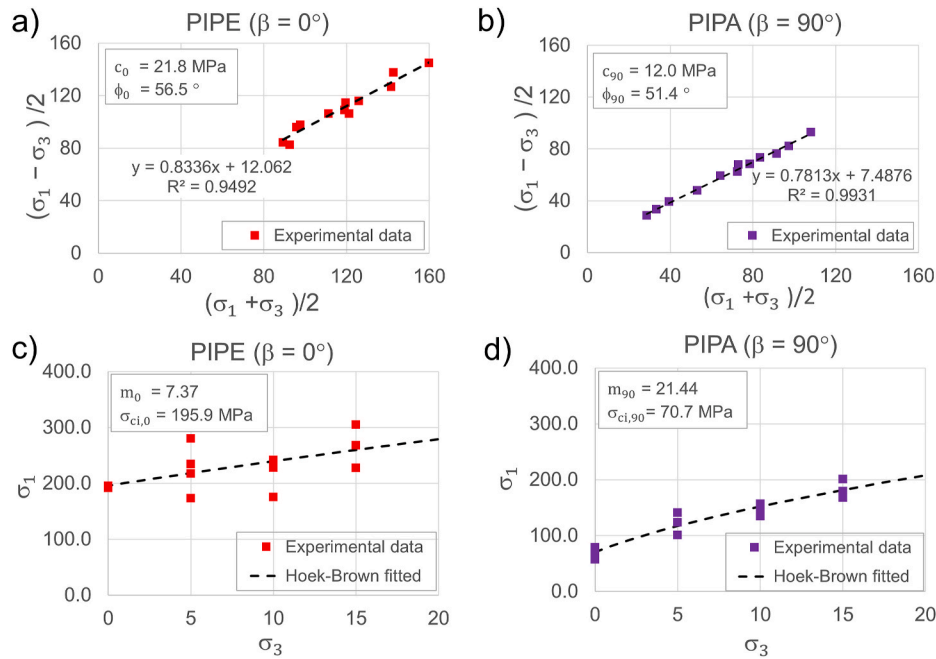


Fig. 13. Determination of intact slate strength parameter for: a) Mohr-Coulomb strength for PIPE ($\beta = 0^\circ$), b) Mohr-Coulomb strength for PIPA ($\beta = 90^\circ$), c) Hoek-Brown strength for PIPE ($\beta = 0^\circ$), and d) Hoek-Brown strength for PIPA ($\beta = 90^\circ$). (For interpretation of the references to color in this figure legend, the reader is referred to the Web version of this article.)

between 45° and 60° . Additionally, in the present experiments, the maximum strength typically occurred for $\beta = 0^\circ$, and there are a significant difference of peak strengths between specimens at $\beta = 0^\circ$ and $\beta = 90^\circ$. It is relevant to note that, for UCS tests of samples with $\beta = 45^\circ$, some tests failed at very low load levels in velocity measurement and stress-strain tests, so some of these low values were not even recorded in some of these cases due to unawareness of the technician. The strength anisotropy ratios, $\sigma_{1,max}/\sigma_{1,min}$, were higher than those of elastic moduli (E/E'). This high strength anisotropy ratios can also be observed for other highly anisotropic rocks, such as Asan Gneiss or Yeoncheon schist.²⁶

First, the uniaxial and triaxial ($\sigma_3 = 5, 10, \text{ and } 15 \text{ MPa}$) experimental data on slates were fit with the Jaeger's plane of weakness (JPW) model,³⁹ resorting to the approach provided by Ambrose.² After that, alternative 2 MC-JPW and 2HB-JPW models are proposed, as potential modifications to the original JPW model, and both of them have been used to fit the experimental data. As described in section 2.2, the JPW model is based on the Mohr-Coulomb criterion, and it has two differentiated mechanisms. The first one associated to intact rock failure and depending on the intact rock parameters of cohesion (c_o) and friction (φ_o). And the second one, where the predominant failure mechanism is associated with the plane of weakness, which depends on the weakness plane strength parameters of cohesion (c_w) and friction angle (φ_w).

In this article, the set of strength parameters (c_o, φ_o, c_w and φ_w) for the JPW model were determined (implemented in a MATLAB code by Ambrose²) by using the minimum root-mean-squared error (RMSE) method. The RMSE values are calculated as shown in Equation (23):

$$RMSE = \sqrt{\frac{\sum_{i=1}^n (P_i - O_i)^2}{n}} \quad (23)$$

where P_i is the predicted value, O_i is the observed value, and n is the number of available tests. The smaller the value of RMSE, the closer the fitted values are to the experimental data. Fig. 12 shows the outcome of the curve-fitting procedure. This graph and Fig. 8 illustrate how specimens with $\beta = 30, 45, 60$ and 75° failed along pre-existing foliation planes, meanwhile, specimens with $\beta = 0$ and 90° failed through intact

rock. Only two strength results were obtained for specimens with $\beta = 15^\circ$, and the JPW model cannot well explain this data. In future research, more experiments would be performed for specimens with $\beta = 15^\circ$.

The JPW model constrains intact rock to exhibit the same peak strength for all foliations dips where the weakness plane does not cause the failure of the sample.³⁹ However, Fig. 12 shows apparent discrepancies of peak strengths for PIPE ($\beta = 0^\circ$) and PIPA ($\beta = 90^\circ$) specimens. This discrepancy is largely consistent with results of experiments and considerations on foliated rocks by Donath,⁴⁷ Amadei⁵⁸ and Akai et al.⁵⁹ (see Fig. 3). Thus, at this point, the JPW model meets one of its limitations to accurately represent observed strength of the slate rocks under scrutiny. Moreover, intact rock strength could vary continuously with the orientation of the weakness planes⁵⁹ and the JPW model is unable to represent this type of behavior.

With the aim of overcoming the above-mentioned drawbacks of the JPW model applied to slaty rocks, an improved approach for theoretical prediction of strength anisotropy is introduced, named 2MC-JPW model (2 Mohr-Coulomb – Jaeger Plane of Weakness). The introduction of this proposal is inspired in empirical evidence and previous studies,^{40,41} where different strength parameters for intact rock are used according to loading direction. Moreover the authors have considered a continuous variation in the strength of the intact rock from $\beta = 0^\circ$ to $\beta = 90^\circ$. This is selected for being a simple hypothesis that consider a smooth variation of strength associated to a transition of failure mechanisms from a typical occurrence of shear banding for $\beta = 0^\circ$ to axial splitting and bulging for $\beta = 90^\circ$, as observed for these cases in tested samples. According to this model, two different failure criteria are combined: (a) for the shear failure mode on the plane of weakness, the same approach as the JPW model is used (see Equation (18) or (19)); whereas, (b) for the failure mode of the intact rock, a β -dependent Mohr-Coulomb failure criterion is proposed, as shown in Equation (24).

$$\sigma_1(\beta) = \sigma_1^0 + \frac{\sigma_1^{90} - \sigma_1^0}{90} \beta \quad (24)$$

In the calibration of the parameters for the 2MC-JPW model, firstly, the strength parameters of specimens with $\beta = 0$ and 90° are determined independently (see Fig. 13a and 13 b), based on fitting a line to strength

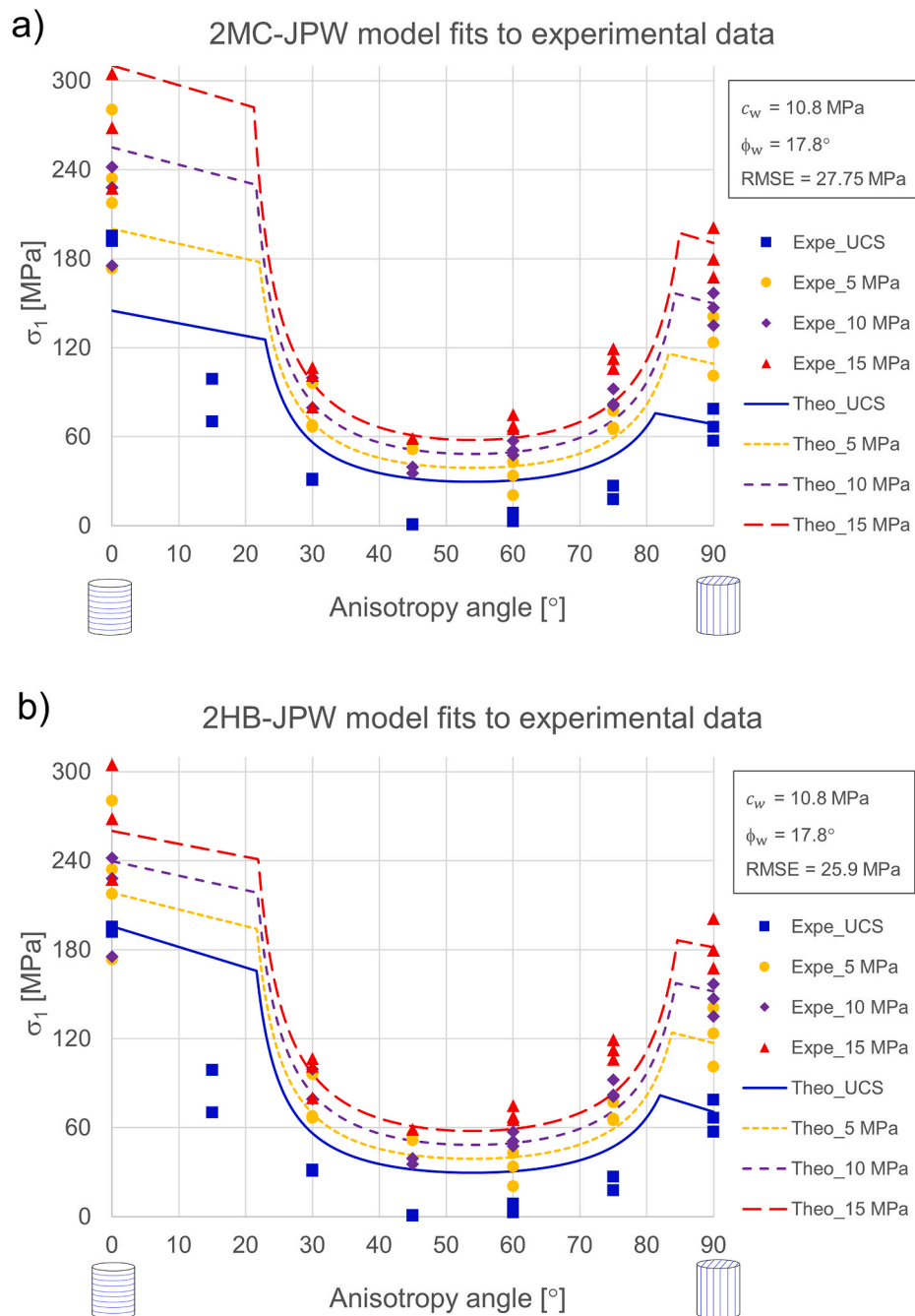


Fig. 14. a) The 2 MC-JPW model fits to experimental data, and b) the 2HB-JPW model fits experimental data. ‘Expe’ and ‘Theo’ in the figure represent experimental data and theoretical solutions, respectively. Strength parameters of PIPE (c_0 and φ_0 for 2MC-JPW model; m_0 and $\sigma_{ci,0}$ for 2HB-JPW model) and PIPA (c_{90} and φ_{90} for 2MC-JPW model; m_{90} and $\sigma_{ci,90}$ for 2HB-JPW model) are presented in Fig. 13.

results in $\tau_m = (\sigma_1 - \sigma_3)/2$, $\sigma_m = (\sigma_1 + \sigma_3)/2$ axes and derivation of cohesion and friction for each case as suggested by Jaeger et al.³⁴ Then, the peak strengths for cases of $\beta = 0$ (σ_1^0) and 90° (σ_1^{90}) can be calculated from Equation (24). After that, the strength parameters (c_w and φ_w) for the plane of weakness were determined by using the minimum root-mean-squared-error (RMSE) method. Note that very few changes had to be introduced in the original MATLAB code by Ambrose² or any alternative method to account for the 2MC-JPW model.

Fig. 14 a shows the outcome of the curve-fitting procedure for the 2MC-JPW model. The RMSE of the 2MC-JPW model is 27.75 MPa, the correctness of prediction has improved by 26.0% compared with the JPW model (RMSE = 37.49 MPa). Although it may be interesting to analyze the influence of different functional forms in Equation (24) for

representing more realistically the strength anisotropy of intact rock, it would require additional laboratory tests and further analysis, exceeding the objectives of this study.

On the other hand and similarly to the 2MC-JPW model, an alternative 2HB-JPW model is proposed. The only difference between the 2MC-JPW and 2HB-JPW model is that the Hoek-Brown standard criterion is used to represent the strength of intact rock in the 2HB-JPW model, by fitting the corresponding σ_{ci} and m Hoek-Brown parameters for intact rock failure for foliation perpendicular and parallel to loading. The empirical Hoek-Brown criterion is not linked to any particular shear failure plane. For many rocks, where the occurrence of failure shear bands is not observed and the strength relations between σ_1 and σ_3 are non-linear, this strength criterion better represents strength results than

Table 3

Root mean square error of predicted values according to different strength approaches in relation to average observed values in the lab according to anisotropy angle levels.

	Anisotropy Angle (°)	Average measured value (MPa)	RMSE JPW	RMSE 2MC-JPW	RMSE 2HB-JPW
PIPE	0	225.5	60.66	49.25	32.32
PI15	15	84.6	53.75	54.93	73.20
PI30	30	75.3	<u>16.15</u>	<u>16.15</u>	<u>16.15</u>
PI45	45	34.6	<u>19.33</u>	<u>19.33</u>	<u>19.33</u>
PI60	60	42.9	<u>13.78</u>	<u>13.78</u>	<u>13.78</u>
PI75	75	76.9	<u>21.31</u>	<u>21.31</u>	<u>21.31</u>
PIPA	90	129.6	49.62	14.56	13.04

the Mohr-Coulomb linear criterion.

Fig. 13c and 13 d shows the determination of strength parameters for specimens with $\beta = 0$ ($m_0 = 7.37$ and $\sigma_{ci,0} = 195.9$ MPa) and 90° ($m_{90} = 21.44$ and $\sigma_{ci,90} = 70.7$ MPa). Remark the significant difference between the values corresponding to the load applied perpendicular and parallel to foliation. Fig. 14 b presents results of the 2HB-JPW model fits to experimental data. The RMSE of the 2HB-JPW model is 25.9 MPa, and the correctness of prediction has improved by 31% and 6.7%, compared with the JPW model (RMSE = 37.49 MPa) and the 2MC-JPW model (RMSE = 27.75 MPa), respectively.

Moreover, the authors have computed the root mean square error associated to different strength approaches for every anisotropy angle, which are compiled in Table 3. While the errors are equal for all approaches when computed for the angles where failure take place through foliation planes (30, 45, 60 and 75°), they significantly differ for 0 and 90°, showing numerically better fits for the 2MC-JPW and 2HB-

JPW approaches, and particularly better, for this last one. Thus, for the slate rock under scrutiny, the 2HB-JPW model shows improved accuracy for representing the actual laboratory strength anisotropic behavior of slates in relation to the JPW model.

Moreover, the authors have fit the JPW and the 2HB-JPW strength models to uniaxial strength test results of Asan gneiss, Boryeong shale and Yeoncheon schist provided by Cho et al.²⁶ The fits of the 2HB-JPW model improve the accuracy of the JPW by a few percentage units of RMSE for the first and third rock results, which will probably not justify the increased complexity of the approach in line with Occam’s razor principle. It will improve though the accuracy of the Boryeong shale strength data by 17%, which could justify using this approach.

5. Discussion

Based on stress-strain testing of a good number of slate samples cut with different orientations of the foliation plane, the anisotropic deformability and strength of this foliated rock have been investigated. The interpretation in terms of observed deformability is given by using the transversely isotropic elastic model, which matches rather well the observed elastic rock sample response.

The strength behavior observed matches the JPW strength model for slate rocks when failure occurs through foliation planes, the most common failure mechanism observed. However, in relation to intact rock strength, two different strength levels were observed for samples cut perpendicular and parallel to foliation respectively. Although this was reflected in the literature in some studies, to the best knowledge of authors there are not commonly accepted strength models able to properly represent this differential strength behavior. This is why the authors have proposed two models based on Mohr-Coulomb and Hoek-

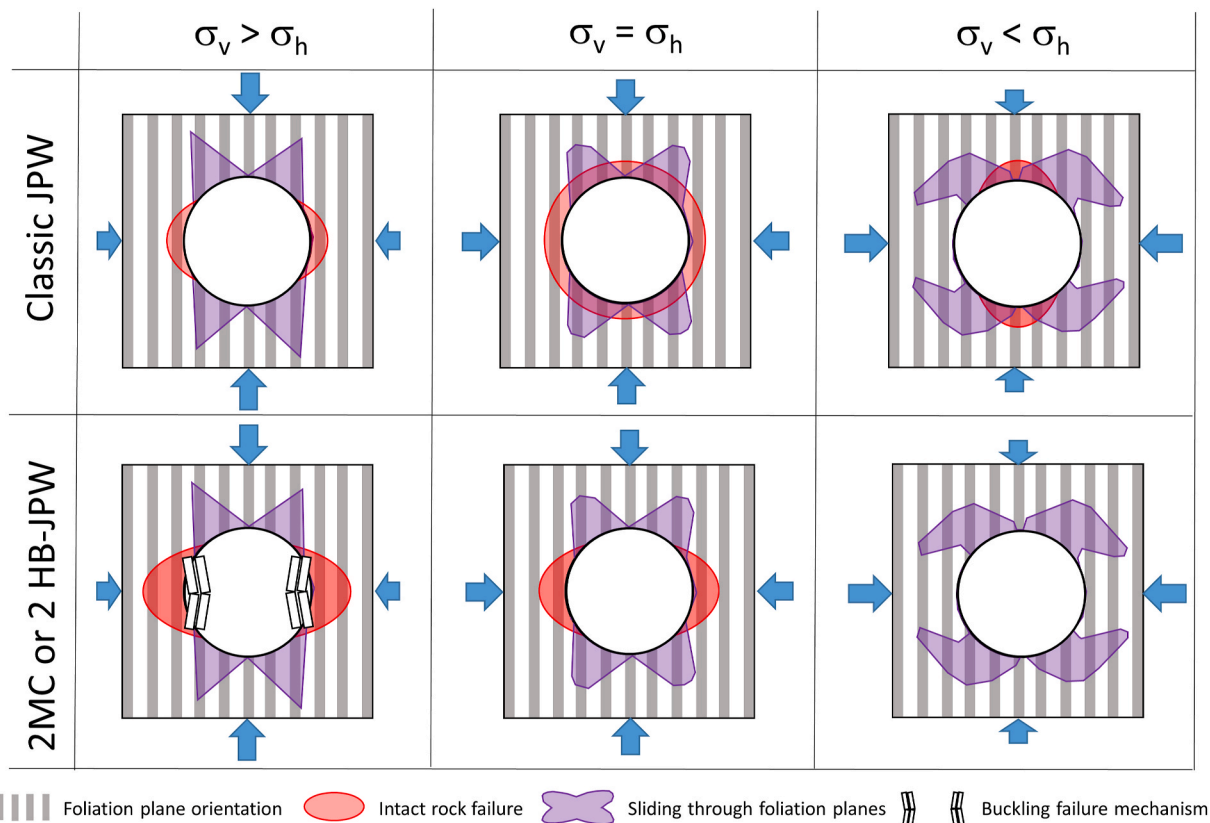


Fig. 15. Rough estimate of plastic zones (in red transparent color) and the sliding foliation zones (in purple colour and estimated with a FEM code) predicted around a hole excavated in a slate-type foliated rock according to three different stress regimes ($\sigma_v > \sigma_h$ in the left column, $\sigma_v = \sigma_h$ in the central column and $\sigma_v < \sigma_h$ in the right column) and different orientations of principal stress in relation to foliation according to the proposed models (2MC-JPW) in the lower row and the JPW model in the upper row. (For interpretation of the references to color in this figure legend, the reader is referred to the Web version of this article.)

Brown intact strength different for every normal direction.

In the alternative proposed models named 2MC-JPW and 2HB-JPW, the intact rock peak strength varies continuously with the orientation of the weakness planes. Compared with the standard JPW model, the proposed 2MC-JPW and 2HB-JPW models are more accurate to predict the observed slate strength results. These models have also shown to be more accurate than standard JPW for other foliated rocks. i.e. Boryeong shale, even if not for every rock of this type.

In this way, when analyzing the mechanical response of a cylindrical hole drilled parallel to foliation, and for the case of an isotropic stress field, the radial stress in the whole periphery will achieve values of twice or more the field stress. If this value is over the uniaxial compressive strength derived from the JPW model, a circular plastic zone will appear around the hole according to this approach. However, if the compressive strength in the directions parallel and normal to foliation differs significantly, the plastic aureole will present an elliptical shape and potentially no failure will be observed in the more resistant hole periphery normal to foliation.

This is illustrated in the central diagrams of Fig. 15. In this diagrams the orientation of foliation is depicted with gray and white stripes, the estimated plastic aureole associated to failure of intact rock is colored in red and the areas with failure through sliding planes derived from anisotropic elasticity and strength models computed with FEM code RS2⁷⁰ are colored in purple.

In the central diagrams of Fig. 15, the cases with isotropic field stress with the corresponding yielded zones are presented for the JPW models in the upper part and for the proposed 2MC-JPW model in the lower part. Equivalent estimates are presented in the left and right hand side columns of this figure corresponding two cases where a moderately anisotropic stress field occurs ($\sigma_1 = 2 \cdot \sigma_3$), according to the direction of the major principal stress in relation to foliation.

Remark how in the lower left diagram of Fig. 15 corresponding to the major principal stress oriented parallel to foliation, the plastic zone significantly increases in the hole sides parallel to foliation and buckling failure phenomena are to be expected, associated to a high stress concentration in the weaker direction of the intact rock. This is only a rough indication of the potential impact of considering the proposed strength approaches to analyze the response of a dry well in slaty rock. Further analyses, which falls out of the scope of this study, are needed to better understand the practical implications of this strength difference that can be relevant for well stability in cases where the breakout limit for the intact rock is higher than that in the foliation planes, in line with studies by Setiawan and Zimmerman.¹⁵

6. Conclusions

Experimental investigation of slates from North-Western Spain was carried out, including analysis of anisotropic deformability and anisotropic strength. Wave propagation velocity results are also included to improve characterization. The transversely isotropic elastic model can reasonably explain the deformability of slates. In calibrating the transversely isotropic elastic parameters, an updated optimization approach was proposed based on considering the first strain invariant as control

parameter, which can improve standard characterization approaches to transversely isotropic elastic constants, particularly when many data are available.

Different failure mechanisms were observed in compression tests on slate samples. A clear difference is observed between failure through weakness planes (for β in the range of 15 to 75°) and failure through intact rock (for $\beta = 0$ and 90°), as otherwise put forward by traditional approaches. However, for the case of the analyzed slates, unlike for some shales, it is also observed that the failure mechanisms for samples cut perpendicular ($\beta = 0^\circ$) and parallel ($\beta = 90^\circ$) to weakness planes tend to differ, appearing buckling phenomena and being the strength systematically smaller for the parallel case.

Through fitting with the experimental data, the Jaeger's Plane of Weakness (JPW) Model can reasonably explain the shear failure behavior on the plane of weakness. However, the JPW model meets one of its limitations in demonstrating the strength of samples cut perpendicular and parallel to foliation angle where failure occurs in the intact rock, which for the case of slates are significantly different.

Thus, to overcome this drawback of the JPW model, in this study, alternative 2MC-JPW and 2HB-JPW models were proposed, such as potential modification of the JPW model when applied to slaty rocks. In both alternative models, the strength of samples normal and parallel to foliation are determined independently, and strength for intact rock is forced to vary continuously with the orientation of the weakness planes. These alternative models are more realistic and they can be helpful to better understand and more accurately simulate the anisotropic strength of slates.

Our results suggest that slates are highly anisotropic materials, and the use of isotropic deformability parameters and failure criteria may produce relevant errors when predicting the mechanical behavior of slates of anisotropic nature. The proposed models will be used to analyze the response of slates in compressive and hydraulic fracture tests. Moreover, they will be implemented in numerical models to assess their reliability when modelling different mechanical tests.

Declaration of competing interest

The authors declare that they have no known competing financial interests or personal relationships that could have appeared to influence the work reported in this paper.

Acknowledgments

The experimental part of this work was funded by REPSOL S.A. The three first authors acknowledge the Spanish Ministry of Universities for funding of the project, awarded under Contract Reference No. RTI2018-093563-B-I00, partially financed by means of ERDF funds from the EU, which permitted to complete the interpretative part of this study. The fourth author acknowledges the CSC scholarship (No. 201706260240) for financing his stay at the University of Vigo, where he was involved in part of this work. Funding for open access charge: Universidade de Vigo/ CISUG.

Appendix. Results of propagation velocity and rock mechanics parameters of tested specimens

Appendix Table 1

Results of tested slate specimens.

	β (°)	V_p (km/s)	V_{s1} (km/s)	V_{s2} (km/s)	σ_3 (MPa)	σ_1^{max} (MPa)	ϵ_y/σ_y (GPa ⁻¹)	ϵ_z/σ_y (GPa ⁻¹)	ϵ_x/σ_y (GPa ⁻¹)
PIPE 1	0	4.84	2.55	2.74	0	191.8	0.026	-0.009	-0.006
PIPE 2	0	4.90	2.03	2.00	0	192.1	0.022	-0.011	-0.010
PIPE 3	0	4.99	2.11	1.97	0	195.4	0.020	-0.003	-0.004
PIPE 7	0	4.59	2.35	2.43	5	234.2	0.034	-0.010	-0.010
PIPE 8	0	4.80	2.23	2.24	2.5	237.8	0.024	-0.011	-0.011

(continued on next page)

Appendix Table 1 (continued)

	β (°)	V_p (km/s)	V_{s1} (km/s)	V_{s2} (km/s)	σ_3 (MPa)	σ_1^{\max} (MPa)	ε_y/σ_y (GPa ⁻¹)	ε_z/σ_y (GPa ⁻¹)	ε_x/σ_y (GPa ⁻¹)
PIPE 9	0	4.89	2.47	2.49	7.5	260.3	0.031	-0.013	-0.011
PIPE 10	0	5.00	2.52	2.50	10	241.9	0.034	-0.010	-0.012
PIPE 11	0	4.94	2.51	2.51	15	268.2	0.025	-0.015	-0.014
PIPE 12	0	5.04	2.46	2.32	12.5	258.5	0.032	-0.019	*
PIPE 13	0	4.97	2.51	2.33	2.5	48.6	-	-	-
PIPE 14	0	4.87	2.13	2.91	2.5	206.9	-	-	-
PIPE 15	0	4.94	2.55	2.52	5	173.5	-	-	-
PIPE 17	0	5.05	2.23	2.54	5	217.7	-	-	-
PIPE 18	0	4.80	2.56	2.45	7.5	202.7	-	-	-
PIPE 19	0	4.92	2.48	2.49	7.5	196.1	-	-	-
PIPE 20	0	4.88	2.55	2.79	10	228.1	-	-	-
PIPE 22	0	4.92	1.76	2.98	10	175.3	-	-	-
PIPE 23	0	4.99	2.48	2.51	2.5	226.2	0.030	-0.011	-0.009
PIPE 24	0	5.04	2.52	2.50	5	280.5	0.019	-0.005	-0.006
PIPE 25	0	4.88	2.55	2.54	15	227.5	-	-	-
PIPE 26	0	4.96	2.51	2.49	15	304.8	*	*	*
PIPA 1	90	6.30	3.06	3.24	0	66.7	0.014	*	*
PIPA 2	90	6.20	3.73	3.73	0	78.7	0.013	*	-0.007
PIPA 3	90	6.19	3.33	3.43	0	57.2	0.030	*	*
PIPA 8	90	6.24	3.74	3.89	2.5	121.7	0.016	*	*
PIPA 9	90	6.23	4.07	3.83	5	101.0	0.010	*	*
PIPA 10	90	6.28	4.43	3.58	7.5	126.1	0.019	-0.002	*
PIPA 11	90	6.26	2.96	3.55	10	156.8	-	-	-
PIPA 12	90	6.24	4.48	3.55	12.5	191.4	0.015	*	*
PIPA 13	90	6.26	3.68	4.33	15	179.6	0.016	-0.003	*
PIPA 14	90	6.26	4.40	3.85	10	147.0	0.012	*	-0.006
PIPA 15	90	6.27	3.78	4.44	2.5	105.0	0.009	*	*
PIPA 16	90	6.26	4.44	4.33	2.5	167.7	0.013	*	-0.005
PIPA 17	90	6.28	3.83	3.80	5	140.8	0.011	*	-0.008
PIPA 19	90	6.24	3.69	4.15	5	123.5	0.011	*	-0.006
PIPA 20	90	6.24	3.74	3.80	7.5	136.0	0.013	-0.005	*
PIPA 21	90	6.23	2.42	3.76	7.5	127.6	-	-	-
PIPA 22	90	6.18	4.39	3.51	7.5	138.1	-	-	-
PIPA 26	90	6.29	3.61	3.71	15	201.0	-	-	-
PIPA 27	90	6.25	4.37	4.34	15	167.7	-	-	-
PIPA 28	90	6.26	3.80	3.81	12.5	173.0	-	-	-
PIPA 29	90	6.25	3.72	3.55	10	134.9	-	-	-
PI15_01	15	4.94	3.19	3.21	0	99.0	0.035	*	-0.003
PI15_02	15	4.95	3.02	2.93	0	70.2	0.020	-0.001	-0.006
PI30_01	30	-	-	-	5	67.6	0.018	-0.001	-0.013
PI30_03	30	-	-	-	5	96.0	0.013	-0.004	-0.003
PI30_04	30	-	-	-	5	66.5	0.028	-0.005	-0.009
PI30_05	30	-	-	-	10	68.5	*	*	*
PI30_06	30	-	-	-	10	99.6	0.015	-0.006	-0.016
PI30_07	30	-	-	-	10	79.4	0.012	-0.004	-0.013
PI30_08	30	-	-	-	15	80.1	-	-	-
PI30_09	30	-	-	-	15	106.6	0.017	-0.005	-0.011
PI30_11	30	-	-	-	15	101.3	0.033	*	-0.008
PI30_16	30	5.23	3.54	3.34	0	30.6	0.055	*	-0.005
PI30_17	30	5.19	3.54	3.45	0	31.5	*	*	*
PI45_01	45	-	-	-	5	51.5	0.006	-0.001	-0.012
PI45_03	45	-	-	-	5	55.4	0.019	-0.003	-0.008
PI45_05	45	-	-	-	10	39.4	0.039	-0.007	-0.008
PI45_09	45	-	-	-	10	35.5	0.016	-0.001	-0.007
PI45_10	45	-	-	-	15	58.9	0.016	-0.002	-0.010
PI45_11	45	5.71	3.34	3.54	0	1.0	*	*	*
PI45_12	45	5.35	3.95	3.84	0	0.5	*	*	*
PI60_01	60	-	-	-	5	33.8	0.013	-0.004	*
PI60_02	60	-	-	-	5	42.9	0.023	-0.005	-0.016
PI60_03	60	-	-	-	5	20.6	0.009	*	-0.007
PI60_04	60	-	-	-	10	47.5	0.007	-0.002	-0.008
PI60_05	60	-	-	-	10	50.8	*	-0.005	-0.010
PI60_06	60	-	-	-	10	57.3	0.013	0.000	-0.003
PI60_07	60	-	-	-	15	65.6	0.011	-0.002	-0.003
PI60_08	60	-	-	-	15	67.5	0.021	-0.001	-0.009
PI60_09	60	-	-	-	15	74.8	0.032	-0.002	-0.009
PI60_14	60	5.68	3.61	3.72	0	3.0	*	*	*
PI60_15	60	5.89	4.38	3.82	0	8.6	*	*	*
PI75_01	75	-	-	-	5	64.9	0.020	*	-0.006
PI75_02	75	-	-	-	5	77.2	0.015	-0.001	-0.003
PI75_03	75	-	-	-	5	66.0	0.013	-0.002	-0.002
PI75_04	75	-	-	-	10	92.2	0.015	-0.003	-0.002
PI75_05	75	-	-	-	10	82.0	0.016	-0.003	-0.003
PI75_06	75	-	-	-	10	81.0	0.013	-0.003	-0.004
PI75_07	75	-	-	-	15	106.2	0.019	-0.002	-0.006
PI75_08	75	-	-	-	15	119.3	0.016	-0.002	-0.006

(continued on next page)

Appendix Table 1 (continued)

	β (°)	V_p (km/s)	V_{s1} (km/s)	V_{s2} (km/s)	σ_3 (MPa)	σ_1^{\max} (MPa)	ϵ_y/σ_y (GPa ⁻¹)	ϵ_z/σ_y (GPa ⁻¹)	ϵ_x/σ_y (GPa ⁻¹)
PI75_09	75	–	–	–	15	112.5	0.008	–0.004	–0.006
PI75_11	75	6.09	4.29	4.26	0	26.9	0.014	–0.003	*
PI75_13	75	6.02	4.66	4.49	0	17.7	0.013	–0.002	*

Note: - Not tested, * Not reliable result.

References

- Hudson JA. The future for rock mechanics and the ISRMS. In: *ISRM International Symposium-5th Asian Rock Mechanics Symposium*. Teheran; 24-26 November 2008: 105–118.
- Ambrose J. *Failure of Anisotropic Shales under Triaxial Stress Conditions*. London: Ph.D. Thesis. Imperial College; 2014.
- García-Guinea J, Lombardero M, Roberts B, Taboada J. Spanish roofing slate deposits. *Trans. Institutions Min. Metall Sect. B Appl. Earth Sci.* 1997;106:205–214.
- Marshak S, Repcheck J. *Essentials of Geology*. third ed. New York: WW Norton & Co; 2009.
- Debecker B, Vervoort A. Experimental observation of fracture patterns in layered slate. *Int J Fract.* 2009;159:51–62.
- Gholami R, Rasouli V. Mechanical and elastic properties of transversely isotropic slate. *Rock Mech Rock Eng.* 2014;47:1763–1773.
- Taboada J, Vaumonde A, Saavedra A, Alejano L. Application of geostatistical techniques to exploitation planning in slate quarries. *Eng Geol.* 1997;47:269–277.
- Sone H, Zoback MD. Mechanical properties of shale-gas reservoir rocks - Part 1: static and dynamic elastic properties and anisotropy. *Geophysics.* 2013;78:381–392.
- Joshi M, Esteban L, Delle Piane C, Sarout J, Dewhurst DN, Clennell MB. Laboratory characterisation of shale properties. *J Petrol Sci Eng.* 2012;88–89:107–124.
- Nasseri MHB, Rao KS, Ramamurthy T. Anisotropic strength and deformation behavior of Himalayan schists. *Int J Rock Mech Min Sci.* 2003;40:3–23.
- Amadei B. Importance of anisotropy when estimating and measuring in situ stresses in rock. *Int. J. Rock Mech. Min. Sci. Geomech.* 1996;33, 293-25.
- Song I, Suh M, Woo YK, Hao T. Determination of the elastic modulus set of foliated rocks from ultrasonic velocity measurements. *Eng Geol.* 2004;72:293–308.
- Alejano LR, Taboada J, Alonso E, Varas F. Modelling & design of an underground room & pillar Mine. In: *Geomechanics/Ground Control in Mining and Underground Construction*. Wollongong; 14-17 July 1998:349–358.
- Sanio HP. Prediction of the performance of disc cutters in anisotropic rock. *Int J Rock Mech Min Sci Geomech Abstr.* 1985;22:153–161.
- Setiawan NB, Zimmerman RW. Wellbore breakout prediction in transversely isotropic rocks using true-triaxial failure criteria. *Int J Rock Mech Min Sci.* 2018;112: 313–322.
- Brown ET, Green SJ, Sinha KP. The influence of rock anisotropy on hole deviation in rotary drilling- A review. *Int J Rock Mech Min Sci.* 1981;18:387–401.
- Wang CD, Tzeng CS, Pan E, Liao JJ. Displacements and stresses due to a vertical point load in an inhomogeneous transversely isotropic half-space. *Int J Rock Mech Min Sci.* 2003;40:667–685.
- Hakala M, Kuula H, Hudson JA. Estimating the transversely isotropic elastic intact rock properties for in situ stress measurement data reduction: a case study of the Olkiluoto mica gneiss. *Finland Int J Rock Mech Min Sci.* 2007;44:14–46.
- Stoeckert F, Molenda M, Brenne S, Alber M. Fracture propagation in sandstone and slate - laboratory experiments, acoustic emissions and fracture mechanics. *J Rock Mech Geotech Eng.* 2015;7:237–249.
- Muñoz-Ibáñez A, Delgado-Martín J, Juncosa-Rivera R, et al. Development of a true triaxial device for hydraulic fracturing experiments. In: *Rock Mechanics for Natural Resources and Infrastructure Development- Proceedings of the 14th International Congress on Rock Mechanics and Rock Engineering*. Foz do Iguaçu; 13-18 September 2019: 1195–1202.
- Muñoz-Ibáñez A, Delgado-Martín J, Costas M, Rabuñal-Dopico J, Alvarellos-Iglesias J, Canal-Vila J. Pure mode I fracture toughness determination in rocks using a pseudo-compact tension (pCT) test approach. *Rock Mech Rock Eng.* 2020;53: 3267–3285.
- González-Molano NA, Alvarellos J, Lakshminantha MR, Arzúa J, Alejano LR. Numerical and experimental characterization of mechanical behaviour of an artificially jointed rock. In: *ISRM International Symposium-EUROCK 2020*. Trondheim; 2020.
- Barla G. Rock anisotropy - theory and laboratory testing. In: Muller L, ed. *Rock Mechanics*. New York: Springer Verlag Wien; 1974:131–169.
- Amadei B. *The Influence of Rock Anisotropy on Measurement of Stresses in Situ*. Berkeley, California: PhD Thesis. University of California; 1982.
- Wittke W. *Rock Mechanics, Theory and Applications v-With Case Histories*. New York: Springer-Verlag; 1990.
- Cho JW, Kim H, Jeon S, Min KB. Deformation and strength anisotropy of Asan gneiss, Boryeong shale, and Yeoncheon schist. *Int J Rock Mech Min Sci.* 2012;50:158–169.
- Lekhnitskii SG. *Theory of Elasticity of an Anisotropic Body*. San Francisco: Holden-Day; 1963.
- Pinto JL. Deformability of schistose rocks. In: *International Society of Rock Mechanics, Proceedings, Belgrade*. vol. 1. 1970:2–30.
- Salamon MDG. Elastic moduli of a stratified rock mass. *Int J Rock Mech Min Sci.* 1968; 5:519–527.
- Chen CS, Pan E, Amadei B. Determination of deformability and tensile strength of anisotropic rock using Brazilian tests. *Int J Rock Mech Min Sci.* 1998;35:43–61.
- Talesnick ML, Bloch-Friedman EA. Compatibility of different methodologies for the determination of elastic parameters of intact anisotropic rocks. *Int J Rock Mech Min Sci.* 1999;36:919–940.
- Worotnicki G. CSIRO triaxial stress measurement cell. In: Hudson JA, ed. *Comprehensive Rock Engineering*. vol. 3. Oxford: Pergamon Press Ltd; 1993:329–394.
- Nejati M, Dambly MLT, Saar MO. A methodology to determine the elastic properties of anisotropic rocks from a single uniaxial compression test. *J Rock Mech Geotech Eng.* 2019;11:1166–1183.
- Jaeger JC, Cook NGW, Zimmerman RW. *Fundamentals of Rock Mechanics*. fourth ed. Oxford and New York: Blackwell Publishing; 2007.
- Saint-Venant B. Sur la distribution des élasticités autour de chaque point d'un solide ou d'un milieu de contexture quelconque. *J Math Pure Appl.* 1863;7–8:353–430.
- Martino D, Ribacchi R. Osservazioni su alcuni metodi di misura delle caratteristiche elastiche di rocce o ammassi rocciosi, con particolare riferimento al problema dell'anisotropia. *L'Industria Mineraria, Ser II.* 1972;23:193–203.
- Alsuwaidi ES, Xi G, Zimmerman RW. Mechanical characterization of Laffan and Nahr Umr anisotropic shales. *J Petrol Sci Eng.* 2021;200:108–195.
- Maia A, Ferreira E, Oliveira MC, Menezes LF, Andrade-Campos A. *Numerical Optimization Strategies for Springback Compensation in Sheet Metal Forming. Computational Methods and Production Engineering*. Woodhead Publishing; 2017: 51–82.
- Jaeger JC. Shear failure of anisotropic rocks. *Geol Mag.* 1960;97:65–72.
- Walsh JB, Brace JF. A fracture criterion for brittle anisotropic rock. *J Geophys Res.* 1964;69:3449–3456, 1964.
- Duveau G, Shao JF, Henry JP. Assessment of some failure criteria for strongly anisotropic geomaterials. *Mech Cohes-Fric Mat.* 1998;3:1–26.
- Ramamurthy T, Venkatappa Rao G, Singh J. A strength criterion for anisotropic rocks. In: *Fifth Australia-New Zealand Conference on Geomechanics, Sydney*. 22-26 August. 1988.
- Bagheripour MH, Rahgozar R, Pashnesaz H, Malekinejad M. A complement to Hoek-Brown failure criterion for strength prediction in anisotropic rock. *Geomech Eng.* 2011;3:61–81.
- Hoek E. Fracture of anisotropic rock. *J South African Inst Min Metall.* 1964;64: 501–518.
- Pariseau WG. Plasticity theory for anisotropic rocks and soil. In: *The 10th US Symposium on Rock Mechanics (USRMS)*. Austin, Texas: American Rock Mechanics Association; 1968.
- Hill R. A theory of the yielding and plastic flow of anisotropic metals. *Proc R Soc London Ser A Math Phys Sci.* 1948;193:281–297.
- Donath FA. Experimental study of shear failure in anisotropic rocks. *Geol Soc Am Bull.* 1961;72:985–989.
- Donath F. Strength variation and deformational behavior in anisotropic rock. In: Judd WR, ed. *State of Stress in the Earth's Crust*. New York: Elsevier; 1964:281–297.
- Donath FA. Faulting across discontinuities in anisotropic rock. Stability of rock slopes. In: *Proceedings of 13th Symposium*. Urbana, Ill. New York: Rock Mech.; 1971: 753–772.
- Mogi K, Igarashi K, Mochizuki H. Deformation and fracture of rocks under general triaxial stress states-anisotropic dilatancy. *J Mater Sci.* 1978;27:148–154.
- Mogi K. Flow and fracture of rocks under general triaxial compression. In: *Proceedings of the Fourth International Congress on Rock Mechanics, Montreal*. vol. 3. 1979:123–130.
- Kwasniewski MA. Mechanical behavior of anisotropic rocks. In: Hudson JA, ed. *Comprehensive Rock Engineering*. vol. 1. Oxford: Pergamon Press; 1993:285–312.
- Mohr O. Welche Umstände bedingen die Elastizitätsgrenze und den Bruch eines Materials. *Z Ver Deut Ing.* 1900:1524–1530.
- Labuz JF, Zang A. Mohr–Coulomb failure criterion. In: *The ISRM Suggested Methods for Rock Characterization, Testing and Monitoring: 2007-2014*. Springer; 2012: 227–231.
- Hoek E, Brown ET. *Underground Excavations in Rock*. London: The Institution of Mining and Metallurgy; 1980.
- Eberhardt E. The Hoek-Brown failure criterion. *Rock Mech Rock Eng.* 2012;45:981.
- Zimmerman RW, Ambrose J, Setiawan NB. Failure of anisotropic rocks such as shales, and implications for borehole stability. In: *ISRM International Symposium-10th Asian Rock Mechanics Symposium*. Singapore: International Society for Rock Mechanics and Rock Engineering; 2018.
- Amadei B. *Rock Anisotropy and the Theory of Stress Measurements*. New York, Tokio: Springer-Verlag; 1983.
- Akai K, Yamamoto K, Ariola M. Experimentelle Forschung über anisotropische Eigenschaften von Kristallinen Schieferen. In: *Proc Rock Mech*. vol. II. 1970:181–186.
- Barton N. Review of a new shear-strength criterion for rock joints. *Eng Geol.* 1973;7: 287–332.
- Maksimovic M. The shear strength components of a rough rock joint. *Int J Rock Mech Min Sci.* 1996;33:769–783.

- 62 ASTM International. *Standard Test Method for Laboratory Determination of Pulse Velocities and Ultrasonic Elastic Constants of Rock*. West Conshohocken, USA: ASTM International; 2004.
- 63 ISRM. *The Complete Isrm Suggested Methods for Rock Characterization, Testing and Monitoring: 1974-2006*. Ankara, Turkey: ISRM Turkish National Group; 2007.
- 64 Akaike H. Information theory and an extension of maximum likelihood principle. In: *Proc. Of the 2nd International Symposium on Information Theory. Budapest*. 1973: 267–281.
- 65 St-Onge A. Akaike information criterion applied to detecting first arrival times on microseismic data. In: *SEG Technical Program Expanded Abstracts 2011*. Society of Exploration Geophysicists; 2011:1658–1662.
- 66 Alejano LR, Arzúa J, Castro-Filgueira U, Kiuru R. reportScale Effect of Intact Olkiluoto Gneissic Rocks through Uniaxial Compressive Testing and Geophysical Measurements. Helsinki: Posiva Oy Report 2018-13.
- 67 Rodríguez Sastre MA, Calleja L. The determination of elastic modulus of slates from ultrasonic velocity measurements. In: *The 10th Congress of the International Association for Engineering Geology and the Environment. Nottingham*. 6-10 September 2006:1–11.
- 68 Ding C, Hu D, Zhou H, Lu J, Lv T. Investigations of P-Wave velocity, mechanical behavior and thermal properties of anisotropic slate. *Int J Rock Mech Min Sci*. 2020; 127:104–176.
- 69 Hoek E, Brown ET. Empirical strength criterion for rock masses. *J Geotech Eng Div*. 1980;106:1013–1035.
- 70 RS2. *2D Geotechnical Finite Element Analysis*. Toronto. Canada: Rocscience; 2021.